ANKARA YILDIRIM BEYAZIT UNIVERSITY

GRADUATE SCHOOL OF NATURAL AND APPLIED SCIENCES

COMPOSITION, STRUCTURE, AND PROPERTY RELATIONSHIP IN CORDIERITE CERAMICS

M.Sc. Thesis by

Merve Şeyma SÜREL

Department of Materials Engineering

November 2024

ANKARA

COMPOSITION, STRUCTURE, AND PROPERTY RELATIONSHIP IN CORDIERITE CERAMICS

A Thesis Submitted to

The Graduate School of Natural and Applied Sciences of

Ankara Yıldırım Beyazıt University

In Partial Fulfillment of the Requirements for the Degree of Master of Science in Materials Engineering, Department of Materials Engineering

by

Merve Şeyma SÜREL

November 2024

ANKARA

M. Sc. THESIS EXAMINATION RESULT FORM

We have read the thesis entitled "**COMPOSITION, STRUCTURE, AND PROPERTY RELATIONSHIP IN CORDIERITE CERAMICS"** completed by **MERVE ŞEYMA SÜREL** under the supervision of **ASSOC. PROF. DR. GÜLSÜM TOPATEŞ** and we certify that in our opinion it is fully adequate, in scope and in quality, as a thesis for degree of Master Science.

Assoc. Prof. Dr. Gülsüm TOPATEŞ

Supervisor

Assoc. Prof. Dr. Şeniz Reyhan KUŞHAN AKIN

Jury Member

Prof. Dr. Hasan OKUYUCU

Jury Member

Prof. Dr. Sadettin ORHAN

Director

Graduate School of Natural and Applied Sciences

ETHICAL DECLARATION

I hereby declare that, in this thesis which has been prepared in accordance with the Thesis Writing Manual of Graduate School of Natural and Applied Sciences,

- All data, information and documents are obtained in the framework of academic and ethical rules,
- All information, documents and assessments are presented in accordance with scientific ethics and morals,
- All the materials that have been utilized are fully cited and referenced,
- No change has been made on the utilized materials,
- All the works presented are original,

and in any contrary case of above statements, I accept to renounce all my legal rights.

Date: **Signature:**

Name & Surname: Merve Şeyma SÜREL

ACKNOWLEDGMENTS

First and foremost, I would like to express my gratitude to my supervisor Assoc. Prof. Dr. Gülsüm TOPATEŞ for her support and guidance since my undergraduate studies. Her sincerity, patience, and invaluable advice made me keep going and achieve many things in my academic life. Without a doubt, she is a significant contributor to my success, and I owe her a great deal of appreciation.

I would like to give special thanks to Res. Asst. İremnur AKÇAKOCA for her endless help and guidance throughout the thesis process. Additionally, I would like to show my gratefulness to Prof. Dr. Cihangir DURAN for his assistance with characterization tests and his insightful advice, which greatly enhanced my research.

I would also like to thank Prof. Dr. Yahya TÜR and the staff at Gebze Technical University for their comprehensive help with flexural strength measurements. My gratitude goes to Dila Su DOMAÇ for her support with dielectric constant measurements. Furthermore, I would like to acknowledge Asst. Prof. Dr. Erdem AKÇA from Sivas Cumhuriyet University for his help with thermal conductivity measurements.

This thesis has been supported by Ankara Yildirim Beyazit University Scientific Research Projects Coordination Unit under grant number FYL-2024-2648.

Last, but not least, my precious parents, my lovely sister and her children, and my dearest friends deserve all the praise and gratitude for supporting me and being there for me all the time.

COMPOSITION, STRUCTURE, AND PROPERTY RELATIONSHIP IN CORDIERITE CERAMICS

ABSTRACT

Cordierite ceramics ($Mg_2Al_4Si_5O_{18}$) are perfect materials for some specific electrical and thermal applications due to their outstanding properties. Having low thermal expansion coefficient and low dielectric constant, high chemical and electrical resistivity make them suitable for extreme condition applications. The effect of composition on the final properties of cordierite is a considerable issue since even minor changes influence the majority of the properties. In this study, four cordierite compositions were chosen from the cordierite region in the phase diagram and their characteristics were observed. The effect of solidus and liquidus temperature on densification and final properties of cordierite ceramics were investigated. The MgO amount was increased to lower these temperatures. Samples were sintered at 1300 and 1350°C. Physical, mechanical, thermal, and dielectric properties were measured and compared with each other. C4 samples with the highest MgO and lowest Al_2O_3 content had the lowest sintering and densification temperature, yet the highest densification. It also had a density of 2.42 g/cm^3, 0.53 percent open porosity, and 1.55 percent closed porosity. Phase analysis proved α-cordierite phase formation as the major phase in all samples. C4 samples showed highest thermal conductivity and thermal diffusivity -which were 1.23 W/m·K and 0.16 mm^2/s, respectively- among the samples as a result of a small amount of open porosity presence. Three-point bending test results indicated that flexural strength of samples varied between 43-73 MPa and they increased with porosity absence. Highest dielectric constant and lowest dielectric loss at 1-5000 kHz frequencies were obtained as 5.2 and 0.003, respectively in the C4 sample. Microstructure and elemental analyses proved the existence of isolated and closed pores and homogeneous elemental distribution in all samples. It was proved that adjusting solidus and liquidus temperatures eliminates an extra melting-quenching process and at 1300°C, cordierite ceramics with the above-mentioned properties can be produced.

Keywords: cordierite, phase diagram, solidus temperature, composition effect, densification, final properties

KORDİERİT SERAMİKLERDE KOMPOZİSYON, YAPI VE ÖZELLİK İLİŞKİLERİ

ÖZ

Kordierit seramikler ($Mg_2Al_4Si_5O_{18}$) öne çıkan özellikleri sebebiyle spesifik elektrik ve ısıl uygulamalar için mükemmel malzemelerdir. Düşük ısıl genleşme katsayısı ve düşük dielektrik sabiti, yüksek kimyasal ve elektrik dayanıklılık kordierit seramiklerin aşırı durumlarda kullanılabilmelerine olanak sağlar. Kompozisyondaki küçük değişimler, özelliklerde büyük değişimlere sebep olduğu için kompozisyonun kordieritin final özelliklerine olan etkisi dikkate alınması gereken bir konudur. Bu çalışmada faz diyagramında yer alan kordierit bölgesinden dört kompozisyon seçilmiş ve özellikleri incelenmiştir. Kordierit seramiklerin katılaşma ve sıvılaşma sıcaklığının, yoğunlaşma ve nihai özellikler üzerine etkisi tez çalışması ile araştırılmıştır. Bu sıcaklıkları düşürmek için MgO miktarı artırılmıştır. Numuneler 1300 ve 1350°C'de sinterlenmiştir. Fiziksel, mekanik, ısıl ve dielektrik özellikler ölçülmüş ve birbirleri ile karşılaştırılmıştır. En yüksek MgO ve en düşük Al_2O_3 içeriğine sahip olan C4 numuneleri, en düşük sinterleme ve yoğunlaşma sıcaklığına sahip olup, en yüksek yoğunlaşmayı göstermiştir. Ayrıca, 2,42 g/cm^3 yoğunluğa, yüzde 0,53 açık porozite ve yüzde 1,55 kapalı poroziteye sahiptir. Faz analizi, mevcut tüm numunelerde ana faz olarak α-kordierit fazının oluşumunu doğrulamıştır. C4 numuneleri, açık porozitenin az olması sebebiyle en yüksek ısıl iletkenlik ve ısıl yayınımını -sırasıyla 1,23 W/m·K ve 0,16 mm^2/s- elde etmiştir. Üç nokta eğme testi sonuçları numunelerin eğilme dayanımının 43-73 MPa arasında değiştiğini ve gözeneklerin yokluğunda arttığını göstermiştir. 1-5000 kHz frekanslarında en yüksek dielektrik sabiti ve en düşük dielektrik kayıp sırasıyla 5,2 ve 0,003 olarak C4 numunelerinde elde edilmiştir. Mikroyapı ve elementel analizler izole ve kapalı gözeneklerin varlığını ve tüm numunelerde homojen elementel dağılımı kanıtlamıştır. Solidüs ve likidüs sıcaklıklarının ayarlanmasının fazladan bir ergime-soğutma sürecini ortadan kaldırdığı ve 1300°C'de yukarıda belirtilen özelliklere sahip kordierit seramiklerin üretilebileceği kanıtlanmıştır.

Anahtar kelimeler: kordierit, faz diyagramı, katılaşma sıcaklığı, kompozisyon etkisi, yoğunlaştırma, nihai özellikler

CONTENTS

ABBREVIATIONS

$2MgO.2Al_2O_3.5SiO_2$	Cordierite
μ	Micro
$2MgO.SiO_2$	Forsterite
$3Al_2O_3.2SiO_2$	Mullite
Å	Angstrom
Al	Aluminum
Al_2O_3	Alumina
AlO_4	Aluminate
B_2O_3	Boric oxide
°C	Degree Celsius
cm^3	Centimeter cube
g	Gram
GPa	Gigapascal
K	Kelvin
kHz	Kilohertz
LiO_2	Lithium oxide
m	Meter
Mg	Magnesium
MgO	Magnesium oxide
Mg(OH)	Magnesium hydroxide
$MgO.Al_2O_3$	Spinel
$MgO.SiO_2$	Enstatite
MHz	Megahertz
min	Minute
mm	Millimeter
mol%	Mole percent
MPa	Megapascal
O	Oxygen
P_2O_5	Phosphorus pentoxide

rpm	Round per minute
Si	Silicon
SiO_2	Silica
SiO_4	Silicate
wt%	Weight percent
α	Alpha
β	Beta

Acronyms

ASTM	American Society for Testing Materials
DI	Deionized
DTA	Differential Thermal Analysis
EDS	Energy Dispersive Spectrometry
MAS	$MgO – Al_2O_3 – SiO_2$
PDF	Powder Diffraction File
SEM	Scanning Electron Microscopy
TCE	Thermal expansion coefficient
TGA	Thermogravimetric Analysis
T_L	Liquidus temperature
T_S	Solidus temperature
XRD	X-ray Diffraction

LIST OF SYMBOLS

%	Percent
°	Degree
A	Specimen area
b	Specimen width
C	Capacitance
C_p	Specific heat
d	Specimen thickness
F_f	Load at fracture
h	Hour
k	Thermal conductivity
L	Distance
Q	Quality factor
tanδ	Loss factor
W	Watt
α	Thermal diffusivity
Δ	Change
ε	Dielectric constant
ε_0	Permittivity of vacuum
ε_r	Relative permittivity
θ	Bragg angle
λ	Wavelength
ρ	Density
σ_{fs}	Flexural strength
Ω	Resistance

LIST OF TABLES

LIST OF FIGURES

CHAPTER 1

INTRODUCTION

1.1 Cordierite Ceramics

1.1.1 Crystal Structure and Polymorphs of Cordierite Ceramics

Cordierite ($Mg_2Al_4Si_5O_{18}$) is one of the ternary compounds within the MgO – Al_2O_3 – SiO_2 (MAS) phase diagram and it stoichiometrically consists of 13.8% MgO, 34.8% Al_2O_3, and 51.4% SiO_2 as seen in Figure 1.1 [1]. Rankin and Merwin first reported it in a study where they worked on the MAS ternary system and revealed the existence of a compound with $2MgO:2Al_2O_3:5SiO_2$ molar ratio, which is cordierite [2]. It melts incongruently at 1465°C resulting in the formation of a new solid phase, mullite, and a liquid [3].

Cordierite is involved in the silicates class within the subgroup of cyclosilicates since it is a magnesium aluminum silicate [4]. Cordierite has 3 polymorphs where two being stable and one being metastable. Stable polymorphs are based on the arrangement order of aluminate (AlO_4) and silicate (SiO_4) tetrahedrons in $(Si_4Al_2)O_{18}$ hexagonal rings. β-cordierite, one of the stable polymorphs, has low symmetry with orthorhombic structure where $(Si,Al)O_4$-tetrahedrons are arranged in an order creating $(Si_4Al_2)O_{18}$ hexagonal rings (Figure 1.2 (a)). The other stable polymorph α-cordierite, also known as indialite, is the high-temperature with hexagonal structure where $(Si,Al)O_4$-tetrahedrons are arranged in a disorder by forming approximate equilateral hexagonal rings (Figure 1.2 (b)). These hexagonal rings are parallel to the c-axis for both orthorhombic and hexagonal structures, and perpendicular to the a and b planes, respectively [4,5]. Table 1.1 summarizes the properties of the cordierite polymorphs.

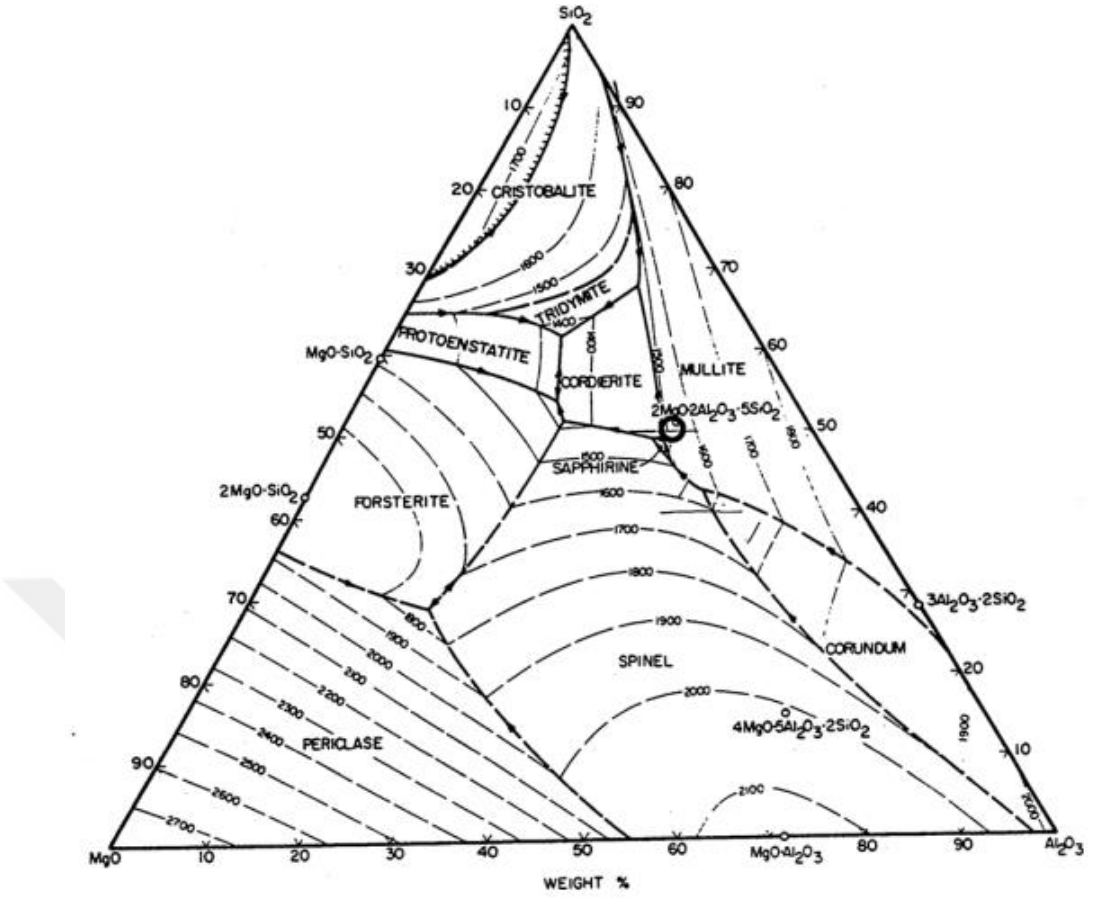

Figure 1.1 MgO – Al_2O_3 – SiO_2 phase diagram [3] where (O) Stoichiometric composition of cordierite

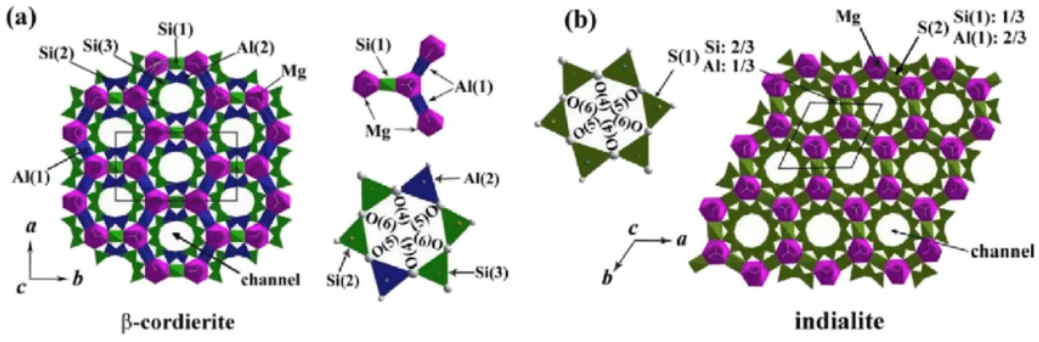

Figure 1.2 Crystal structure of (a) β-cordierite, (b) α-cordierite [5]

Table 1.1 Properties of the cordierite polymorphs [4,5]

Properties	**α-cordierite (indialite)**	**β-cordierite**	**μ-cordierite**
Crystal structure	Hexagonal	Orthorhombic	Rhombohedral
Crystallization range	1000-1300°C	< 950°C	< 925°C
Classification (depending on stability)	Stable between 1450-1460°C	Below 1450°C	Metastable
Classification (depending on distortion index (Δ))	High cordierite	Low cordierite	β-quartz solution

1.1.2 Production Methods of Cordierite Ceramics

During the synthesis of cordierite ceramics, the reaction between SiO_2, Al_2O_3, and MgO in the raw materials causes cordierite formation as a result of phase transformation. α-cordierite can be produced from the direct reaction of initial oxides, the reaction of compounds and intermediate phases, and transformation of μ to α [6].

Synthesis of cordierite ceramics can be performed via several methods. Whereas conventional methods such as solid-state sintering and glass crystallization are the most common techniques to produce cordierite ceramics, chemical methods such as sol-gel, and other methods such as combustion sintering, spray pyrolysis, precipitation, foaming, spark plasma sintering, additive manufacturing, hydrolysis, and Pechini method are also used in the cordierite ceramic production [6–10].

1.1.3 Properties of Cordierite Ceramics

Cordierite ceramics feature with its high thermal and electrical properties. They possess low thermal expansion coefficient (TCE) depending on phase composition and amount, and low dielectric constant among the ceramic materials. The thermal conductivity of cordierite is low compared to the other materials. The chemical and thermal stability of cordierite ceramics are superior as well as thermal shock resistance and electrical resistivity allowing them to be used in high-temperature applications and extreme conditions [11]. However, cordierite ceramics have low density compared to other ceramic materials due to large voids in cordierite structure and challenging production. Thus, the mechanical properties of them are inferior. Also, cordierite ceramics have a narrow sintering range in which high sintering temperatures are required. Controlling the cordierite composition is a challenge during the sintering process so, it must be conducted carefully. These difficulties in the cordierite sintering result in poor densification [1,9]. The numeric properties of cordierite ceramics are listed in Table 1.2.

Table 1.2 Properties of cordierite ceramics [11–13]

Properties	Values
Melting point (°C)	1465
Density (g/cm^3)	2.0 – 2.53
Thermal expansion coefficient between 25-1000°C (K^{-1})	$1.4 – 2.6 \times 10^{-6}$
Thermal conductivity (W/m·K)	2.50
Dielectric constant (ε)	4 – 6
Young's modulus (GPa)	139 – 150
Flexural strength (MPa)	80 – 90
Electrical resistivity (Ω·cm)	$\rho > 10^{12}$
Thermal shock resistance (ΔT)	> 350 K

1.1.4 Application Areas of Cordierite Ceramics

As a result of having low dielectric constant and low thermal expansion coefficient, cordierite ceramics are mainly used in electrical-electronic and thermal applications. They are mainly used as microelectronics, radome, catalysts, integrated circuit boards, ceramic membranes, thermal shock-resistance tableware, thermal and electrical insulators, porous ceramics, and microwave dielectric resonators [9,10,14]. Also, thanks to their high thermal and chemical stability, they are used as molten metal filters, catalyst carriers for automobile exhaust systems, heat exchangers for gas turbines, and refractory material for kiln furnaces [9,11]. Some cordierite application examples can be seen in Figure 1.3 [15]. With the improvement in mechanical and electrical properties, the application area of cordierite ceramics can be widened.

Figure 1.3 Cordierite applications: molten metal filter, radome, and refractory (from left to right) [15]

1.2 Phase Diagrams

1.2.1 MgO – Al_2O_3 – SiO_2 System

Phase diagrams, also termed as equilibrium diagrams, represent the relations between different phases under equilibrium conditions, based on three external parameters – temperature, composition, and pressure [16,17]. They allow to control the phase structure of a specific system [17]. The systems involving three components are known as ternary systems.

The MgO – Al_2O_3 – SiO_2 system is also a ternary phase diagram. It consists of many components that are used as commercial products. The binary side MgO – Al_2O_3

includes spinel ($MgO.Al_2O_3$) which can be used as substrate material for circuits and refractory applications. The binary side Al_2O_3 – SiO_2 contains alumina, silica, and mullite ($3Al_2O_3.2SiO_2$) which are refractory compounds. MgO – SiO_2 binary side involves enstatite ($MgO.SiO_2$) and forsterite ($2MgO.SiO_2$) which are used as electrical insulators (steatite ceramics) and furnace lining materials, respectively. Cordierite ($2MgO.2Al_2O_3.5SiO_2$) is a ternary compound present in this system and it can be used for various applications mentioned in section 1.1.4 [18]. MgO – Al_2O_3 – SiO_2 ternary system can be seen in Figure 1.4.

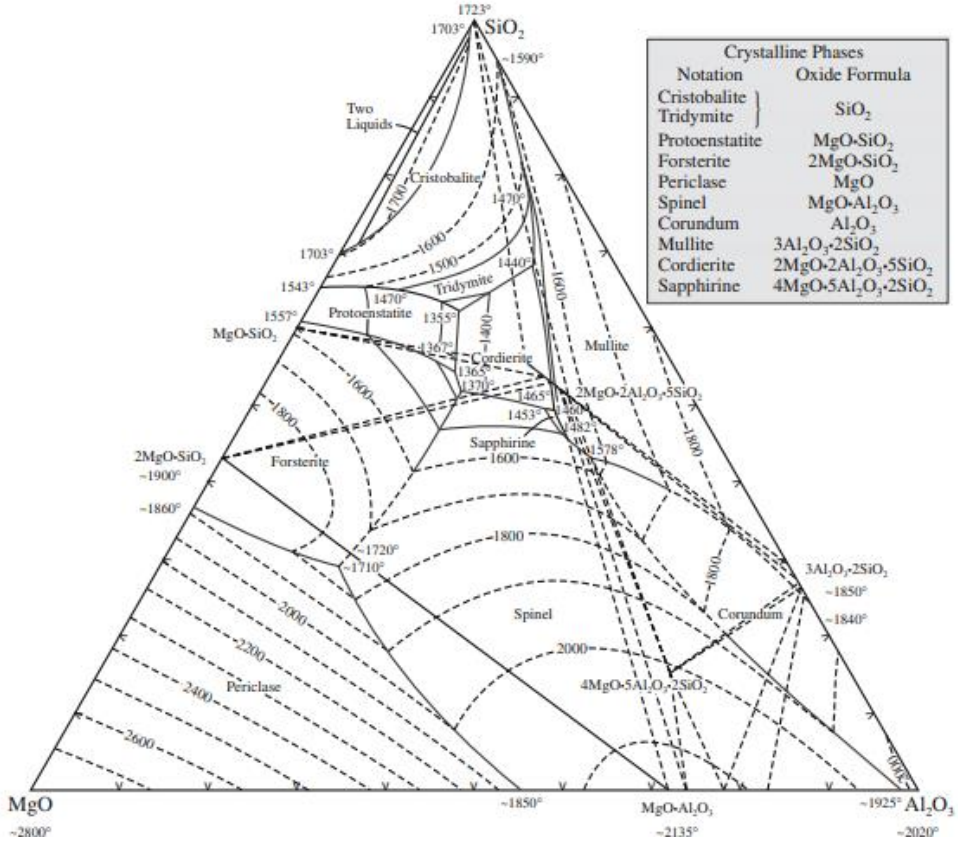

Figure 1.4 The MgO – Al2O3 – SiO2 ternary system [19]

1.2.2 Effect of T_S and T_L in Sintering

Solidus and liquidus temperatures are the borders in the phase diagrams. Solidus temperature is the temperature below which no liquid exists. All phases below the solidus temperature are solid and completely crystalline. Above liquidus temperature,

no crystal can occur and all phases above the liquidus temperature are entirely liquid. At liquidus temperature, crystals first begin to form when the melt is cooled under equilibrium conditions. To increase the sintering temperature range of materials, T_S and T_L differences must be high. Also, as the liquidus temperature decreases, the sintering temperature of the material is lowered which provides less energy usage and more efficiency [18,20].

1.3 Effect of Composition on Cordierite Properties

In the literature, there are limited numbers of research studying the effect of composition on cordierite properties.

Xu et. al. studied the effect of the MgO/SiO_2 ratio and Al_2O_3 amount on crystallization behavior, thermal expansion coefficient, and microstructure of the cordierite glass-ceramics. Samples were prepared from pure commercial oxides and sintered via the powder sintering method. Different characterization techniques were applied to observe the effect of MgO/SiO_2 ratio and Al_2O_3 amount. Results showed that increasing the MgO/SiO_2 ratio provided less effect on decreasing the liquid viscosity and melting temperature than decreasing Al_2O_3 content. According to the DTA results, MgO/SiO_2 ratio governed the cordierite crystallization because of liquid absence at low temperatures whereas Al_2O_3 dominated the crystal growth at higher temperatures due to its influence on reducing the liquid viscosity. Low thermal expansion coefficient was obtained from the samples whose composition was close to the stoichiometric composition and absent in terms of quartz. Higher Al_2O_3 content caused mullite formation. Phase separation with interconnected structures was obtained where in compositions with lower MgO/SiO_2 ratio and Al_2O_3 content. Also, the lowest porosity was observed in the samples with lowest Al_2O_3 content [21].

Li et. al. studied the effect of excess MgO mole ratio on the sintering process and the properties of cordierite ceramics. Kaolin, magnesium carbonate, magnesium oxide, and attapulgite were used as starting materials and the samples were sintered with the solid-state method between 1100 and 1300°C. XRD and SEM analyses were

performed. According to the results, the cordierite phase formation started at 1200℃ and its crystallization increased with increasing temperature. The samples sintered at 1300℃ showed the highest shrinkage, lowest porosity, and highest density compared to the 1100 and 1200℃. As the MgO mole ratio increased, the shrinkage percentage rose too. It is revealed that the excess MgO was not able to decrease the crystallization temperature, yet it triggered the liquid phase formation. The pore-forming effect of the basic magnesium oxide was lost when it was added excessively which means when the mole ratio of MgO was over a limit, the sample condenses immediately [22].

Li et. al. fabricated dense cordierite ceramic by reducing the Al_2O_3 content. Samples were produced from kaolin, basic magnesium carbonate, and attapulgite and sintered at 1200℃. Cordierite phase formation was observed with a minor phase of sapphirine. As the Al_2O_3 mole ratio reduced, porosity also decreased while bulk density and shrinkage increased. The best Al_2O_3 mole ratio for cordierite ceramic production was considered as 1.4 [23].

Soltan et. al. produced cordierite briquettes and cordierite-based co-clinkers in order to observe the effect of phase composition and microstructure on the thermal expansion coefficient and electrical properties. Samples were produced by natural raw materials and fired at different temperatures. The liquid amount during the firing process was calculated via $MgO – Al_2O_3 – SiO_2$ ternary system. They concluded that direct use of developed raw materials provided cordierite phase formation whose peaks intensified with increasing temperatures. Co-clinker compositions with the lowest Al_2O_3 content showed maximum bulk density among the other samples. Also, they proved that cordierite briquettes can be used as insulators in electronic applications due to their dielectric constants and loss factors. As the corundum phase increased in cordierite briquettes, it dominated the composition and cordierite content decreased causing in higher thermal expansion coefficient [9].

Banjuraizah et. al. investigated the effect of excess MgO on dielectric properties and thermal expansion coefficient in non-stoichiometric cordierite glass ceramics. Kaolin, talc, α-alumina, silica, and magnesia were used as starting raw materials. Cordierite compositions were prepared by glass crystallization method melting raw

materials in alumina crucibles at 1500℃ and quenching the melt. As a result, excess MgO in cordierite glass-ceramic compositions caused a decrease in crystallization temperature and thermal expansion coefficient whereas dielectric constant and dielectric loss increased [24].

Banjuraizah et. al. observed the effect of excess MgO in stoichiometric cordierite composition on crystallization and transformation of phases. α-cordierite was produced via the glass crystallization method by using kaolin and talc. Results showed that as the MgO mole ratio increased, the crystallization temperature decreased, and μ-cordierite formation was delayed. They revealed that low-purity raw materials promoted to decrease in sintering and crystallization temperature. Above a specific amount of MgO, α-cordierite intensity decreased as a result of forsterite formation. MgO dissolved in grains to produce minor phases instead of acting as a nucleation agent and sintering aid [25].

de Almeida et. al. studied cordierite from different compositions containing talc, kaolin waste, and magnesium oxide aiming to use it in insulating and refractory applications. Results showed that the particle size and sintering temperature can affect the cordierite formation process. Cordierite nucleation began at 1250℃ and more intense peaks were obtained at 1350℃. Rose-like microstructure was observed in the compositions containing kaolin waste and magnesium oxide. In the composition involving talc, hexagonal tube-like morphology was detected. Also, kaolin was accepted as a beneficial raw material which is environmentally friendly and reduces cost [10].

Hwang et. al. investigated the effects of composition on the formation of different phases and microstructures in cordierite glass ceramics. Sintered samples were characterized by different methods. Results showed that the compositions with higher $MgO\text{-}SiO_2$ content than stoichiometric cordierite compound inhibited the formation of μ-cordierite but promoted the α-cordierite crystallization which resulted in higher α-cordierite content. In the microstructural analysis, it was observed that the dendrites of μ-cordierites had thick arms. Contrarily, compositions richer in Al_2O_3 than stoichiometric composition had no influence on the crystallization of α-cordierite. Hence, α-cordierite formed after the majority of glass crystallized to μ-

cordierites causing the lesser amount of α-cordierite. The dendrites of μ-cordierites had thinner arms [26].

Zu et. al. examined the effect of composition on crystallization, mechanical properties, crystallization kinetics, and viscosity of glass fibers and MgO-Al_2O_3-SiO_2 based high-strength glasses. SiO_2 and Al_2O_3 contents remained constant while (LiO_2/B_2O_3)/MgO ratio varied. Results showed that, with the increasing (LiO_2/B_2O_3)/MgO ratio crystal growth in the glass was suppressed. Cordierite phase formation was observed over 1000℃. Produced fibers showed higher tensile strength and Young's modulus over commercial E-Glass fibers [27].

Hu et. al. studied the crystallization kinetics of P_2O_5 – B_2O_3 containing cordierite-based glasses by using non-isothermal differential thermal analysis (DTA). Glasses with higher SiO_2 and Al_2O_3 content among other compositions provided higher activation energy for crystallization. In addition to the α-cordierite, several minor phases such as forsterite, clinoenstatite, and farringtonite were obtained in completely crystallized samples. It is revealed that the crystallization behavior of powdered glass was dominated by the surface crystallization mechanism which does not depend on the composition [28].

1.4 Motivation

This study mainly aims to produce high-density cordierite ceramics by lowering the sintering temperature by using information from the $MgO - Al_2O_3 - SiO_2$ ternary phase diagram.

There are a limited number of studies about the investigation of cordierite ceramics based on compositional effects in the literature, to the best of our knowledge. In this study, the relationship between compositions, structures, and properties of cordierite ceramics will be observed. Herein, new cordierite compositions will be determined with the help of the MAS phase diagram. Thanks to the specific determination from the ternary system, widening the sintering temperature range and lowering the sintering temperature are targeted. As a result of all these parameters, cordierite ceramics with high density, improved thermal and electrical properties, and higher strength are planned to be produced.

In case of achieving the dense cordierite ceramics sintered at lower temperatures, densification behavior, phase formation, microstructural development, mechanical (hardness and flexural strength), dielectric (dielectric constant and dissipation), and thermal (thermal conductivity) properties will be investigated and reached results will be evaluated.

CHAPTER 2

EXPERIMENTAL PROCEDURE

2.1 Determination of the Composition

Four cordierite compositions were determined by using $MgO – Al_2O_3 – SiO_2$ ternary phase diagram in order to observe the effect of starting composition on the final properties of cordierite. T_S and T_L differences were kept high, and various locations were chosen as much as possible when compositions were designed. Compositions were named as C1, C2, C3, and C4 regardless of their location in the phase diagram. C2 composition represents the stoichiometric composition whereas the others are situated in three different compatibility triangles which are $SiO_2 – 2MgO.2Al_2O_3.5SiO_2 – MgO.SiO_2$ (C1 composition), $SiO_2 – 2MgO.2Al_2O_3.5SiO_2 – 3Al_2O_3.2SiO_2$ (C3 composition), and $MgO.SiO_2 – 2MgO.2Al_2O_3.5SiO_2 – 2MgO.SiO_2$ (C4 composition). The compositions and molar ratios, T_S and T_L values, and their positions in the cordierite region belonging to the $MgO – Al_2O_3 – SiO_2$ ternary phase diagram can be seen in Table 2.1, Table 2.2, and Figure 2.1, respectively.

Table 2.1 Cordierite compositions

Composition	Weight (%)			Molar Ratio (%)		
	MgO	**Al_2O_3**	**SiO_2**	**MgO/Al_2O_3**	**MgO/SiO_2**	**SiO_2/Al_2O_3**
C1	14.02	30.95	55.03	0.45	0.25	1.78
C2	13.78	34.86	51.36	0.40	0.27	1.47
C3	12.76	34.23	53.02	0.37	0.24	1.55
C4	23.39	23.39	53.22	1.00	0.44	2.28

Table 2.2 T_S and T_L values of compositions

Composition	$T_{Liquidus}$ (°C)	$T_{Solidus}$ (°C)
C1	1480	1355
C2	1510	1440
C3	1580	1440
C4	1390	1365

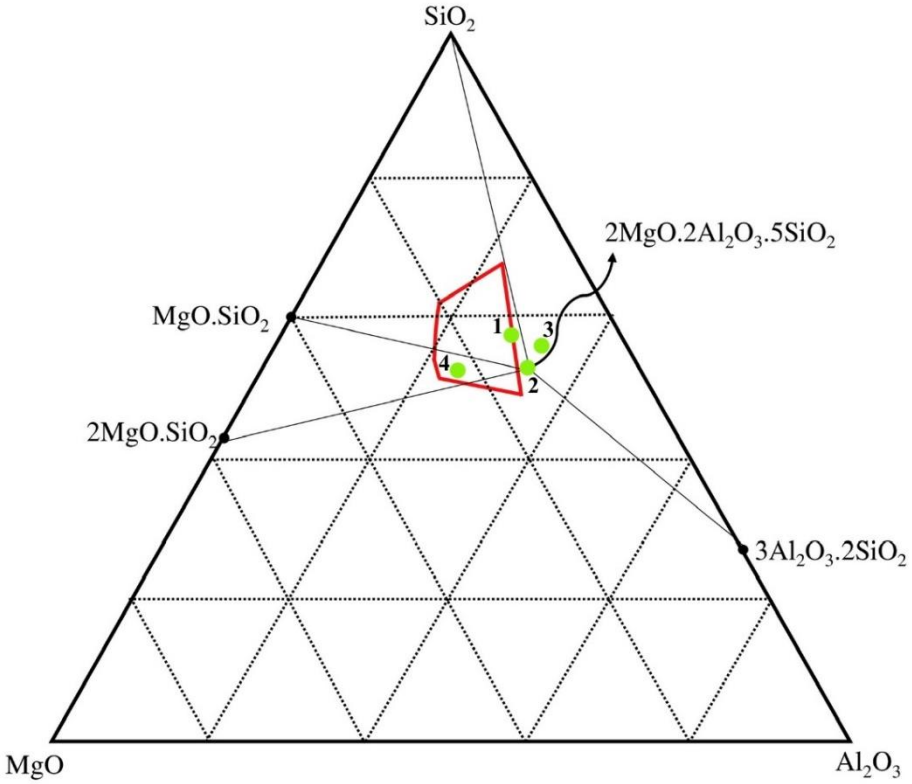

Figure 2.1 Schematic representation of the location of compositions on MgO – Al_2O_3 – SiO_2 ternary phase diagram

2.2 Sample Preparation

2.2.1 Powder Preparation

Pure oxides were used during the preparation of powder mixtures. Silica (SiO_2, 10μm, 99.9% purity, Ege Nanotek, Türkiye), aluminum oxide (Al_2O_3, ≥98% purity, Honeywell Fluka), and magnesium oxide (Nano MgO, Merck) were used as raw materials. First, the microstructures of the oxide powders were observed (Figure 2.2). MgO showed a leaflike microstructure with micron-size particles as seen in Figure 2.2 (a). Al_2O_3 powder had a platelike microstructure and bigger particles than other powders as represented in Figure 2.2 (b). SiO_2 was not homogeneous and had particles with different shapes and sizes. The particle size distribution of silica was wide, as shown in Figure 2.2 (c).

SiO_2, Al_2O_3, and MgO were weighed as 25 g in total, according to the compositions given in Table 2.1. 50 g of DI water, 0.12% amount of ammonium polyacrylate (Darvan 821-A) as dispersing agent, and zirconia balls were added as media to the polyethylene container. The powder mixture was subjected to ball milling for 24 h with 165 rpm in order to obtain a homogeneous mixture. The slurries dried at 45°C in a drier for a week and after that, they were ground by mortar and sieved.

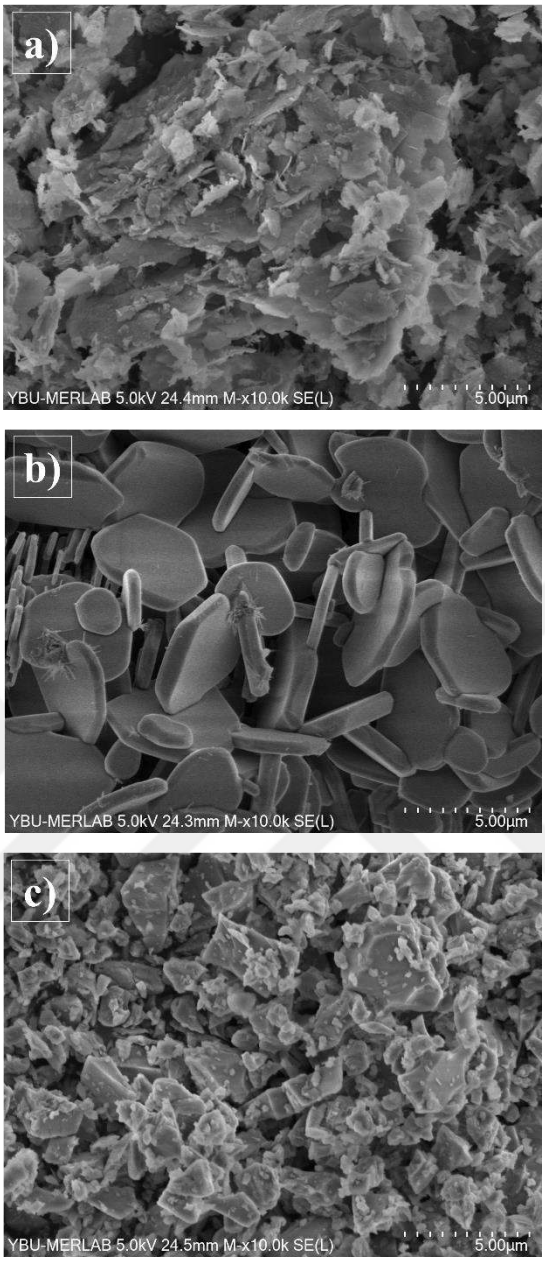

Figure 2.2 Microstructures of raw materials (a) MgO, (b) Al_2O_3, and (c) SiO_2

2.2.2 Shaping and Sintering of the Samples

All four powder mixtures were pressed into 2 cm-diameter pellets at 25 MPa by using a uniaxial press (MSE Teknoloji, Türkiye). For the three-point bending test, powders were pressed at 20 MPa via a rectangular prism die with approximately 3 by 4 by 50 mm dimensions as indicated in ASTM C1161 – 18 [28].

The samples were sintered at both 1300℃ and 1350℃ with a 5℃/min heating and cooling rate and dwelt at those temperatures for 3 h according to the performed thermal analysis and the literature.

2.3 Physical, Mechanical, and Electrical Characterization

2.3.1 Density Measurement

The bulk densities and open porosities of sintered samples were measured via the Archimedes' method. Firstly, sintered samples were weighed (W_1) and then boiled in DI water for 2 h in order to fill all the open porosities. After that, samples were weighed as suspended in the water by the Archimedes' system (W_2). Finally, they were weighed again after removing all the water from the sample surfaces (W_3). The values were calculated according to the following formulas where Equation 2.1 for bulk density and Equation 2.2 for apparent porosity [1].

$$\text{Bulk density} = \frac{W_1}{W_3 - W_2} \times \text{The density of water} \quad (2.1)$$

$$\text{Apparent porosity (\%)} = \frac{W_3 - W_1}{W_3 - W_2} \times 100 \quad (2.2)$$

where W_1 is sintered weight (g), W_2 is suspended weight (g), and W_3 is saturated weight (g).

The closed porosity of samples was calculated according to the following equations.

$$P_c = P_t - P_o \quad (2.3)$$

where P_c is closed porosity of the sample, P_t is the total porosity of the sample, and P_o is the apparent porosity of the same sample. Total porosity, P_t, can be calculated from following formula.

$$P_t = \left(1 - \frac{\rho_b}{\rho_t}\right) \times 100 \quad (2.4)$$

where ρ_b is the bulk density of material (g/cm^3) whereas ρ_t is the true density of the material (g/cm^3).

2.3.2 XRD Analysis

The phase determination of the sintered samples was operated via X-ray Diffractometer (XRD) device (Rigaku, MiniFlex-600) under 40 kV and 15 mA. The analyses were conducted with Cu Kα radiation (λ = 1.5418Å). The scanning was held in a range of $5° < 2\theta < 60°$ with 2°/min scan rate and 0.02° step size.

2.3.3 SEM Analysis

Microstructural analyses were performed via Scanning electron microscope (Hitachi, Su5000) by coating the samples with gold. Also, elemental analyses of samples were conducted by EDS detector (Oxford, X-MaxN 80).

2.3.4 3-Point Bending Strength Measurements

The rectangular prism samples were used to measure the flexural strength by the 3-point bending test. For this process, a universal testing machine (Instron 5569, 500 kg load cell) were performed with 40 mm of span length and 0.5 mm/min crosshead speed. The test was conducted according to the ASTM C1161-18 standard [29]. The flexural strength of the samples was calculated according to the following formula [17]:

$$\sigma_{fs} = \frac{3 \times F_f \times L}{2 \times b \times d^2} \qquad 2.5$$

where σ_{fs} is flexural strength (MPa), F_f is the load at fracture (N), L is the distance between the supports, b is the specimen width (mm), and d is the specimen thickness (mm).

2.3.5 Dielectric Constant and Dissipation Factor Measurements

Capacitance measurements of the samples were conducted in order to investigate the dielectric properties. One side of the samples were coated with Ag paste and first dried at room temperature. Then they were heated to 150℃ and the same procedure

applied to the other sides of the samples. The analyses were done at 1 kHz, 10 kHz, 100 kHz, 1 MHz, and 5 MHz at room temperature by using an impedance analyzer (Hioki, IM3570). The capacitance values and the dissipation factors were achieved from the device. The dielectric constants were calculated according to the following formula [30]:

$$K = \varepsilon_r = \frac{C \times d}{\varepsilon_0 \times A} \quad 2.6$$

$$Q = \frac{1}{tan\delta} \quad 2.7$$

where K or also ε_r is the dielectric constant or also the relative permittivity, C is capacitance (F), d is the specimen thickness (m), ε_0 is the permittivity of vacuum (F/m) which equals to 8.854 x 10^{-12} F/m, and A is the area of specimen (m^2) for Equation 2.6 and Q is the quality factor and tanδ is the loss factor for Equation 2.7.

2.3.6 Thermal Analysis

Thermal conductivity, thermal diffusivity, and heat capacitance measurements were performed by Hot Disk method via thermal property measurement device (Hot Disk, TPS 3500). C5465 sensor was used during the analysis while r = 3.189 and red cable were used. The thermal conductivities of the samples were calculated according to the following equation [30]:

$$k = \alpha \times \rho \times C_p \quad 2.8$$

where k is thermal conductivity (W/m.K), α is thermal diffusivity (m^2/s), ρ is density of samples (kg/m^3), and C_p is specific heat (J/kg.K).

Moreover, TG-DTA analysis of samples was conducted via simultaneous thermal analyzer (Netzsch STA 449 F3) with 20 °C/ 5.0 min in order to understand thermal behavior of the cordierite samples.

2.3.7 Optic Dilatometer and Heat Microscope

The sintering behavior was analyzed using an optical dilatometer (MISURA ODHT HSM 1600/80). Heat treatment was performed in two stages. Firstly, the green samples were first fired at 500°C with a heating rate of 80 °C/min and then sintered at 1450°C with 10°C/min heating rate.

CHAPTER 3

RESULTS AND DISCUSSION

3.1 Effect of Composition on Densification

Samples sintered at 1300°C showed different behavior from each other. C4 densified completely at 1300°C whereas C1, C2, and C3 could not complete the densification process. At 1350°C, compositions C1, C2, and C3 densified as desired. However, C4 samples melted and stuck to the refractory. Therefore, following sintering processes continued as this information.

Table 3.1 summarizes the densification behavior of cordierite ceramics. Despite a 50°C lower sintering temperature, C4 having the lowest solidus and liquidus temperature, showed the highest bulk density value with nearly zero open porosity, 0.53%. Also, its isolated porosity amount was calculated as 1.55%. For all compositions, density values tended to diminish with an increase in solidus and liquidus temperatures. Since an excess amount of MgO was used to lower the solidus and liquidus temperatures, the effect of this oxide was investigated. Banjuraizah et al. concluded the effect of MgO on densification and crystallization of α-cordierite in glass-ceramic form. With the addition of MgO, Si-O bonds are broken, and non-bridging O is formed. It accompanies a reduction in the sintering temperature and accelerates densification. Also, disruption of atomic arrangement eases the crystallization of α-cordierite [24]. In another study, Li et. al. revealed that excess MgO mole ratio promotes liquid production and densification process during the cordierite ceramic production. Additionally, they achieved that as the MgO content increase, the amount of firing shrinkage increases as well [22]. Same behavior was obtained in the current study. C4, having the highest MgO amount, showed highest shrinkage ratio among the compositions while C3 with the lowest MgO content had the lowest firing shrinkage ratio. Moreover, T_L influences the firing shrinkage. As T_L increases, firing shrinkage decreases. Figure 3.1 explains the relationship between T_L and firing shrinkage ratio. Besides, the weight loss ratios also were in direct proportion with MgO content and shrinkage ratios.

The Al_2O_3 influenced the bulk density, and the amount of apparent porosity as expected. As the Al_2O_3 content increased, apparent porosity ratio increased whereas bulk density values decreased as in Figure 3.2. Xu et. al. revealed that an increase in Al_2O_3 mole ratio rises water absorption and porosity of the samples whereas bulk density decreases [21]. Several studies in the literature also supports this phenomenon [9,23].

Table 3.1 Densification behavior of samples

Composition	Weight Loss (%)	Firing Shrinkage (%)	Bulk Density (g/cm^3)	Open Porosity (%)
C1	7.48 (± 0.02)	14.56 (± 1.71)	1.97 (± 0.02)	21.77 (± 1.16)
C2	7.30 (± 0.10)	10.68 (± 0.42)	1.75 (± 0.02)	32.59 (± 0.67)
C3	6.61 (± 0.03)	10.64 (± 0.88)	1.78 (± 0.00)	32.15 (± 0.21)
C4	13.71 (± 0.84)	21.90 (± 0.46)	2.45 (± 0.00)	0.53 (± 0.12)

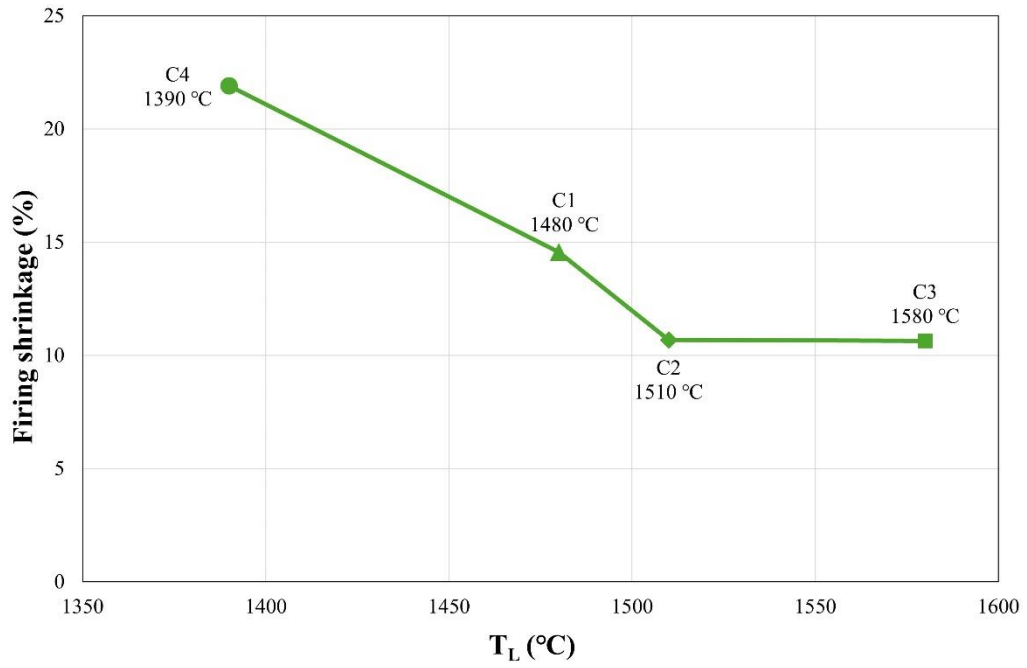

Figure 3.1 The effect of T_L (°C) on firing shrinkage

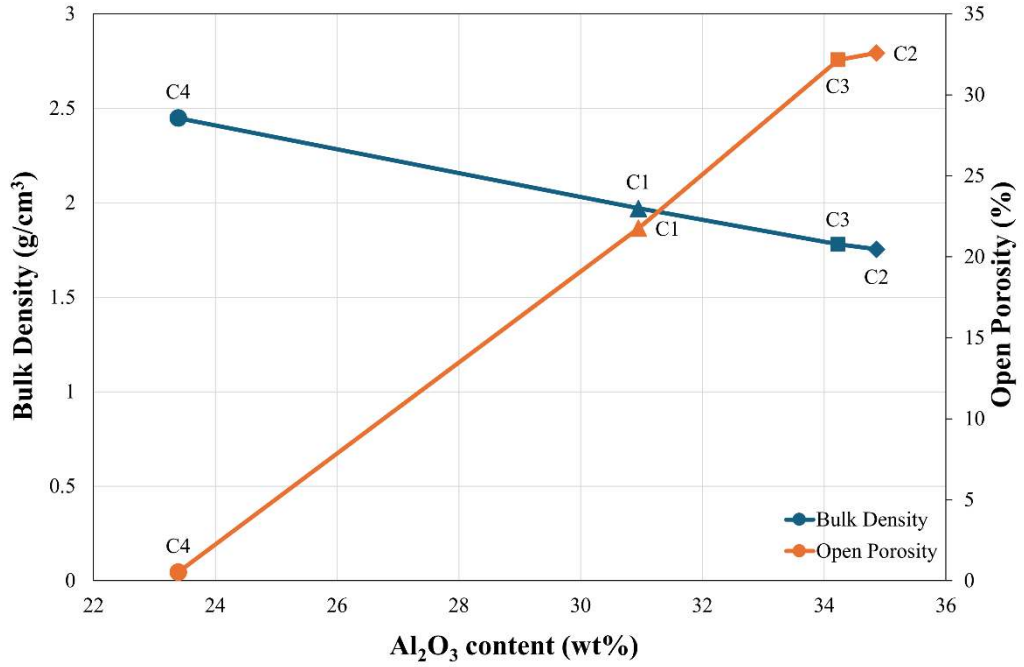

Figure 3.2 Bulk density and open porosity vs Al_2O_3 content

Deformation-temperature curves from optical dilatometer are given in Figure 3.3. Three distinct regions were observed for all compositions. A rapid deformation rate was seen in the first region (gray region) around 1140°C showing the densification of samples has been started. For C1, the deformation ratio was 19%, C2-C3 was 16.5% and as expected the highest deformation was obtained for C4 with 30% where the highest density was achieved. Densification finished for C1 at 1250°C, shifted 10°C higher in C2-C3. Densification was completed at 1270°C in C4. The deformation became constant for all samples in the second region (pink region) which can be attributed to crystallization. To have full density, it is important to finish consolidation before the crystallization since the formation of crystal phases increases the viscosity of the liquid phase and obstructs densification [24,27]. Crystallization finished earlier in C4 at 1420°C and a sudden decrease in deformation occurred due to the melting of the composition. The highest melting temperatures belonged to C2 and C3. It can be seen from Figure 3.4 (a) that the temperatures of maximum shrinkage rates are in the following order C4 (1158°C), C2-3 (1240°C) and C1 (1190-1260°C). This proves the effect of liquidus temperatures on the densification of samples. During the sintering, C4 was melted at 1350°C, so the sintering temperature of this composition was reduced to 1300°C. Melting

temperatures from the phase diagram and optical dilatometer differed significantly from the sintering condition. Since phase diagram is constructed under equilibrium conditions, providing these conditions during the production process is impossible. A higher heating rate was applied in dilatometric analysis than the rate used in the sintering process. As the rate is increased, the critical temperatures such as glass transition, melting are shifted to higher temperatures. Karamanov showed that a rise in the rate from 2°C/min to 30°C/min, the densification was postponed to 100°C higher temperature [31].

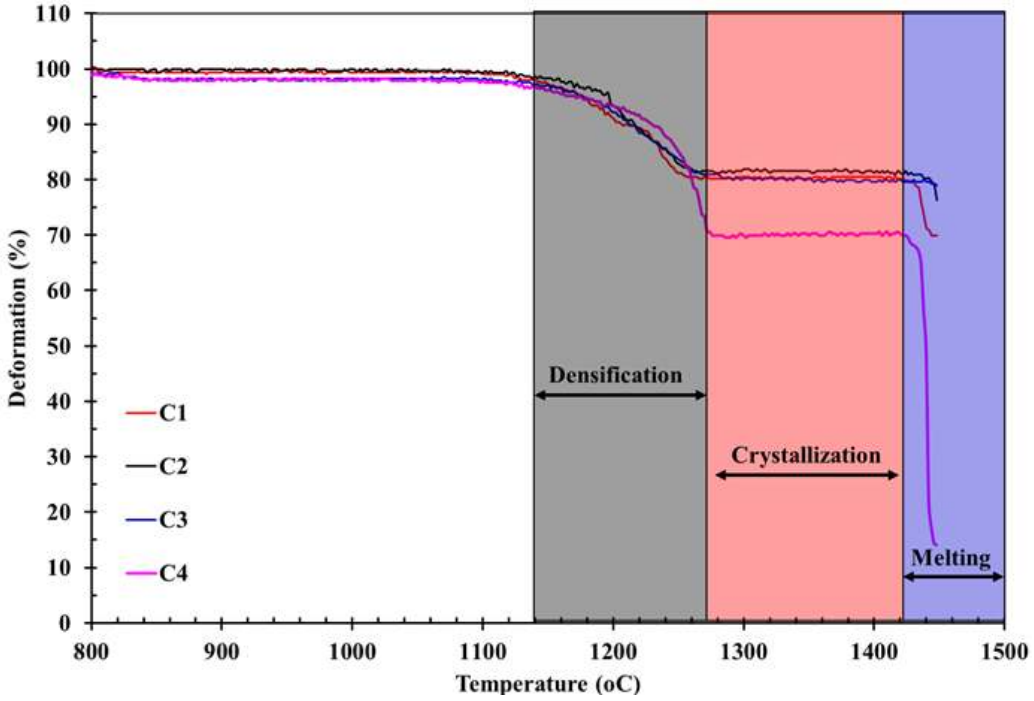

Figure 3.3 Deformation (%) of compositions

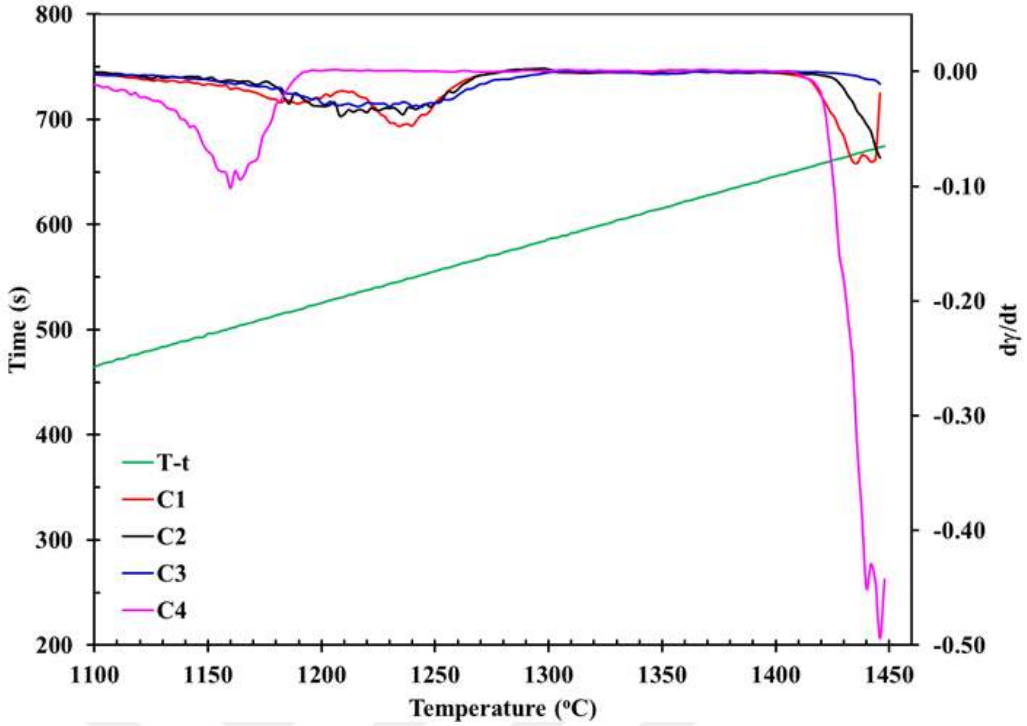

(a)

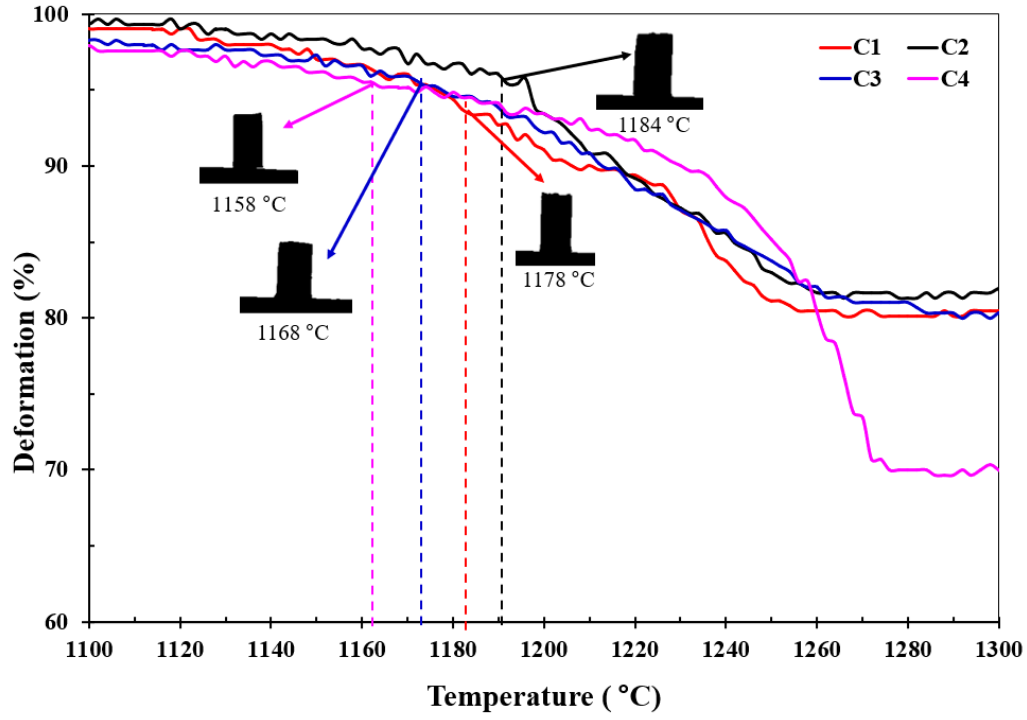

(b)

Figure 3.4 (a) Shrinkage rate of compositions and time-temperature curve of analysis between 1100 °C to 1500 °C, **(b)** Deformation (%) of compositions between 1100 °C to 1300 °C

The sintering temperatures of the samples were indicated by hot stage microscopy and the images of the samples at these temperatures can be seen in Figure 3.5. As coinciding with the other results, C4 had the lowest sintering temperature, 1158℃. The softening, sphere, half sphere, and fusion images could not be captured due to the extremely high heating rate. Samples degraded very fast, and these stages were not detected. Lao et. al. stated that with the excess MgO content, flow and hemispherical temperatures decreased [32]. As a degradation was observed in all samples, it can be said that liquid phase amount was abundant and liquid phase sintered took place [21].

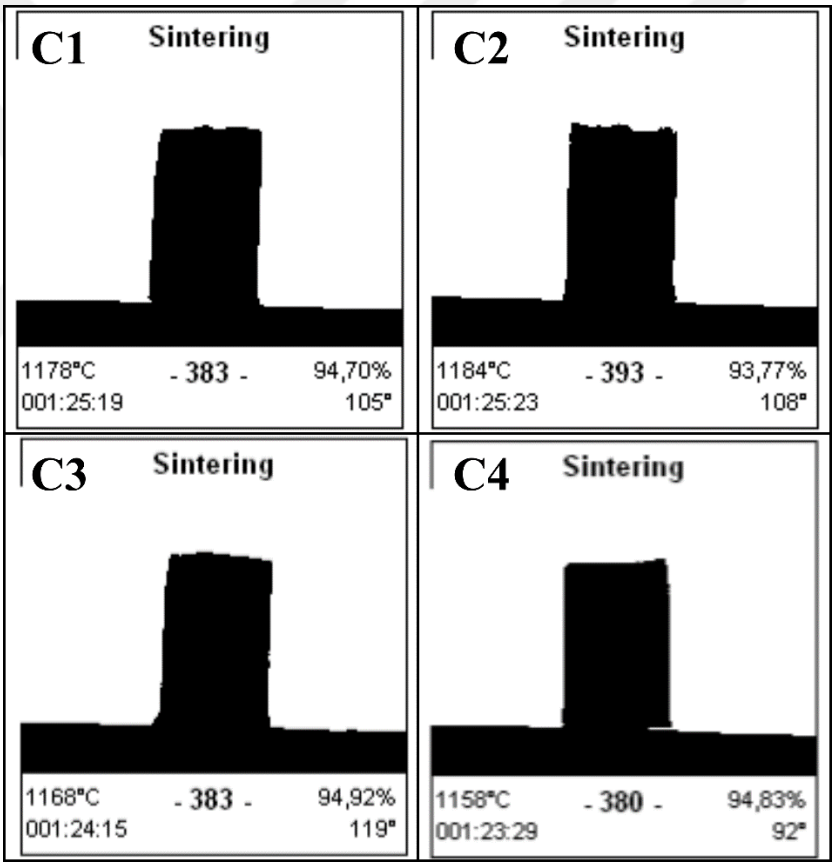

Figure 3.5 Hot stage microscopy images

3.2 Effect of Composition on Phase Development

3.2.1 Thermal Analyses

TG-DTA were performed up to 1400 °C and only C4 melted below this temperature confirming the experimental procedure. According to the TGA results shown in Figure 3.6 (a), the highest mass loss occurred in C4 samples with approximately 10%. The mass loss in C1, C2, and C3 came after C4 and was in the range of 6-8 %. DTG analysis showed an endothermic peak at 376.9 °C which was the dehydroxylation of magnesium hydroxide which formed during the ball milling process due to the reaction between nano MgO and water [33]. DTA curves of the compositions can be seen in Figure 3.6 (b). The endothermic peak at 574 °C corresponds to the polymorphic transition of quartz from α to β. According to the literature, milling may cause a decrease in this area [34]. The exothermic peak formed at 831 °C belongs to the enstatite phase and it is the first exothermic reaction in the DTA curve [6]. The sharpness of this peak is slightly higher in C4 composition than others. This might be caused by the high amount of MgO content in C4 composition. For compositions C1, C2, and C3, mullite formation was observed between 1150-1250 °C. Lamara et. al. stated that mullite, cristobalite, and sapphirine formation takes place at this temperature range [35]. However, in the DTA curve of C4, sharp endothermic and exothermic peaks were present. At 1253 °C, SiO_2 transition took place, and β-quartz transforms to μ-cordierite. The exothermic peak at 1336 °C corresponds to α-cordierite formation [6]. Only for C4 composition, melting below 1400 °C can be seen. The variation between thermal analyses and sintering process resulted from the different furnace and device conditions.

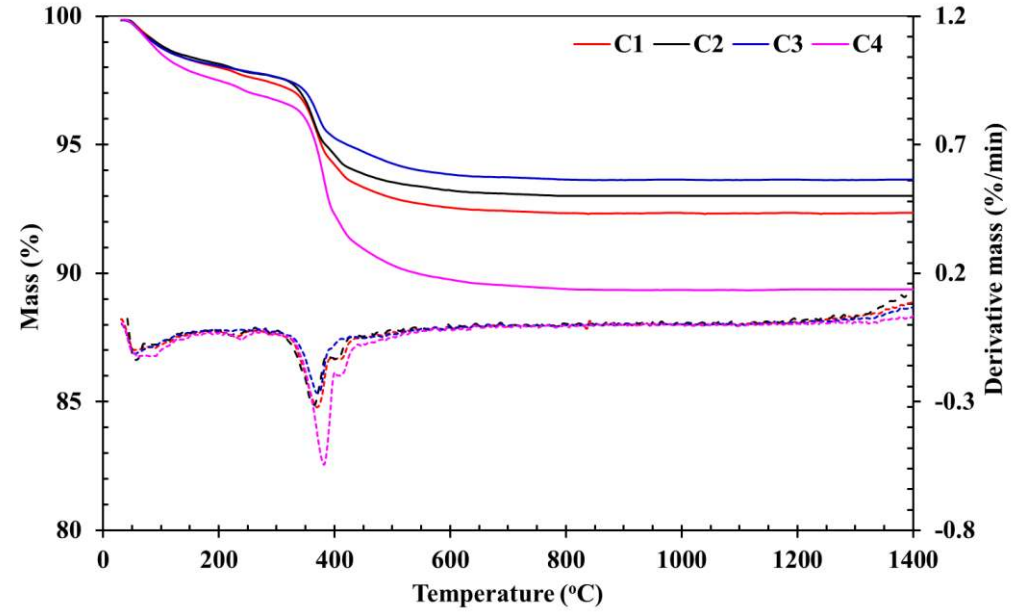

(a)

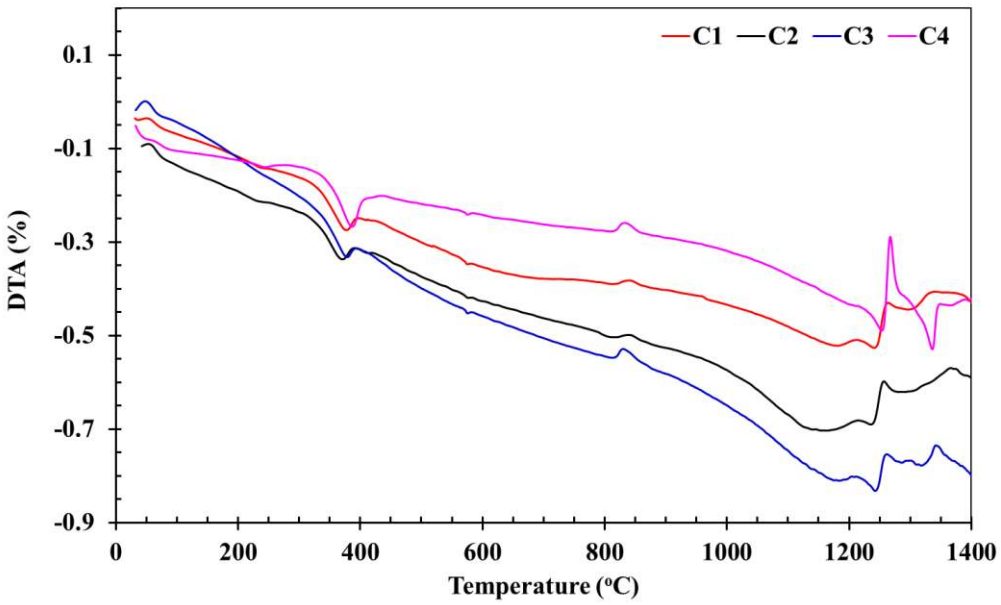

(b)

Figure 3.6 (a) Thermogravimetric (TG) analysis**, (b)** Differential thermal analysis (DTA) of compositions C1, C2, C3, and C4

3.2.2 XRD Measurements

The XRD patterns of C1, C2, and C3 compositions at 1350℃ and C4 composition at 1300℃ are given in Figure 3.7. All compositions showed the indialite (α-cordierite) formation ($2MgO.2Al_2O_3.5SiO_2$, PDF Card No.: 01-089-1485). The peak intensities of C1, C2, C3 appeared similar to the first two sharpest peak at 2θ=10.45° and 2θ=29.50°, in order whereas the first two sharpest peak of the C4 was the opposite of it. When the composition effect on cordierite phase formation was reviewed in the literature, it was found that in a study where Li et. al. observed the influence of Al_2O_3 content in cordierite ceramics, the intensity of the peak at 2θ=10.45° increased with the increasing amounts of Al_2O_3 mole ratio and became the sharpest peak. On the other hand, the intensity of the peak at 2θ=29.50° decreased with an increasing Al_2O_3 content and became the second sharpest peak [23]. In the current study, the intensity of the peak at 2θ=10.45° was higher than the peak at 2θ=29.50° for C1, C2, and C3 whose Al_2O_3 content was higher than C4. As the Al_2O_3 content decreased, the peak intensity at 2θ=10.45° lowered and the peak at 2θ=29.50° became the most intense peak.

Corundum (Al_2O_3, PDF Card No.: 00-046-1212) appeared as secondary phase in C1, C2, and C3 samples while it was not present in C4 samples. This situation may arise due to the scarcity amount of Al_2O_3 in C4 composition since it contained the least amount of alumina among the compositions. Mullite ($2Al_2O_3.2SiO_2$, PDF Card No.: 00-001-0613) formation was observed in C1, C2, and C3 where it mainly appeared in C2. This can be explained with excess MgO in C4 composition as the amount of Al_2O_3 and SiO_2 were higher in the other compositions than C4. Sapphirine ($4MgO.5Al_2O_3.2SiO_2$, PDF Card No.: 00-019-0750) occurred as secondary phase in C4 samples. Li et. al. indicated that sapphirine appeared at samples with higher MgO ratios [22,23]. In C4 samples, the sapphirine phase formed due to excess amount of MgO than other compositions. There was no evidence about the sapphirine formation in C1, C2, and C3 compositions as a result of lower MgO mole ratio. Highly weak forsterite ($2MgO.SiO_2$, PDF Card No.: 01-075-1446) peaks showed up as minor phases in all samples.

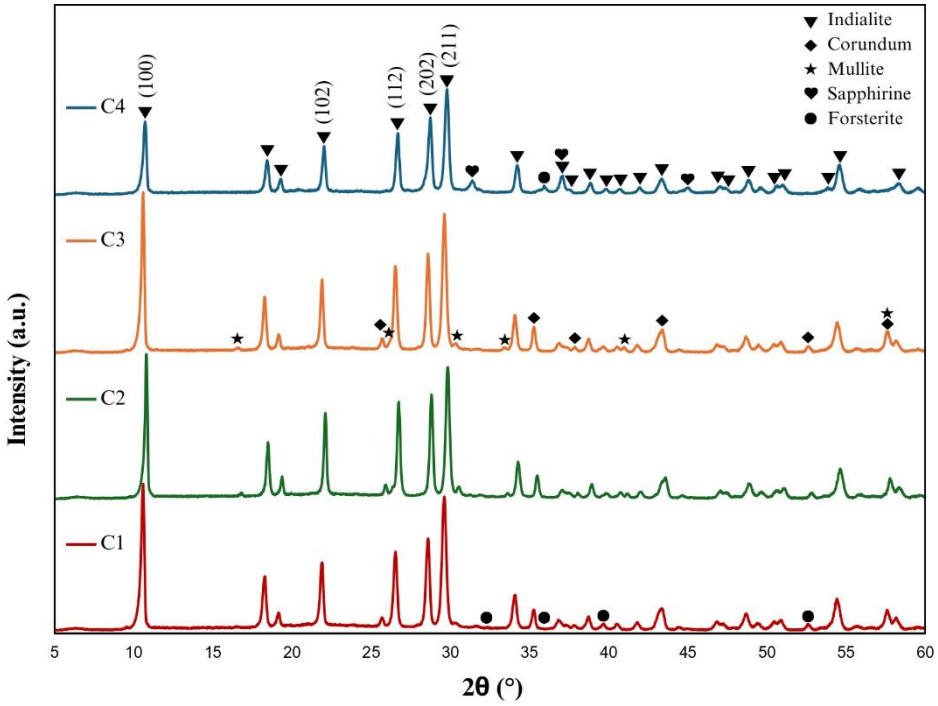

Figure 3.7 XRD patterns of C1, C2, C3 (1350°C) and C4 (1300°C)

3.3 Effect of Composition on Thermal, Mechanical, and Dielectric Properties

Thermal conductivity values of the samples were calculated according to the given equation, and they were listed in Table 3.2. Figure 3.8 shows the comparison of compositions in terms of apparent porosity and thermal conductivity. C1, C2, and C3 showed thermal conductivity values close to each other being in sequence with apparent porosity values. Due to the high apparent porosity percentage in these samples, the thermal conductivity values were low. C4 with lower porosity showed higher thermal conductivity than others. Lao et. al. explained the relation between MgO content, open porosity, and thermal conductivity in cordierite ceramics. As the MgO mole ratio increased, liquid viscosity decreased whereas the amount of liquid content increased causing the formation of closed pores and lessen of open pores. Hence, increase in MgO content and decrease in apparent porosity amount caused a rise in thermal conductivity value [32]. This situation can also be explained by the porosity increase, heat transmission is prohibited by air whose thermal conductivity is very low, 0.022 W/m·K [36]. In this study, same sequence was observed, when the

MgO content increased, open porosity decreased, and thermal conductivity raised as represented in Figure 3.9.

However, the obtained thermal conductivity values were extremely low compared to the literature studies. Garcia et. al. measured the thermal conductivity of commercial porous cordierite ceramic burners with 50 and 40 vol % porosity. They concluded that the thermal conductivity values ~0.4 W/m·K and ~0.6 W/m·K for 50 vol% and 40 vol% porous burners, respectively [37]. Similarly, in another study Li et. al. investigated the thermal conductivity of cordierite ceramics with porosity ranging 85.4-87.8%. They found that gel-casted samples possessed thermal conductivity of ~0.217 W/m·K [38]. In the current study, cordierite ceramics whose open porosity amount was between 0.27-27.26% had thermal conductivity between 0.31-1.23 which was incoherent with the literature.

Thermal diffusivity is the ability of a material to spread heat. Thermal diffusivity of a material decreases with porosity presence. Garcia et. al also observed the thermal diffusivity of porous commercial cordierite burners with 40 and 50 vol% open porosity. They measured the thermal diffusivity ranging between 0.004-0.006 cm^2/s and 0.005-0.008 cm^2/s for samples with 50 vol% porosity and 40 vol% porosity, respectively [37]. Lao et. al. also proved that as the porosity decreased, thermal diffusivity increased as well. Thermal diffusivity values ranged between 1.24-1.49 mm^2/s for cordierite ceramics with 14-24% porosity amount [32]. However, in this study the diffusivity values were extremely lower than the ones in the literature. The values ranged between 0.02-0.16 mm^2/s for cordierite ceramics with 0.27-27.26% porosity.

Table 3.2 Comparison of the thermal conductivity and thermal diffusivity values

Samples	Thermal conductivity (W/m·K)	Thermal diffusivity (mm^2/s)
C1	0.34 (± 0.01)	0.02 (± 0.00)
C2	0.31 (± 0.02)	0.04 (± 0.05)
C3	0.31 (± 0.02)	0.01 (± 0.00)
C4	1.23 (± 0.05)	0.16 (± 0.03)

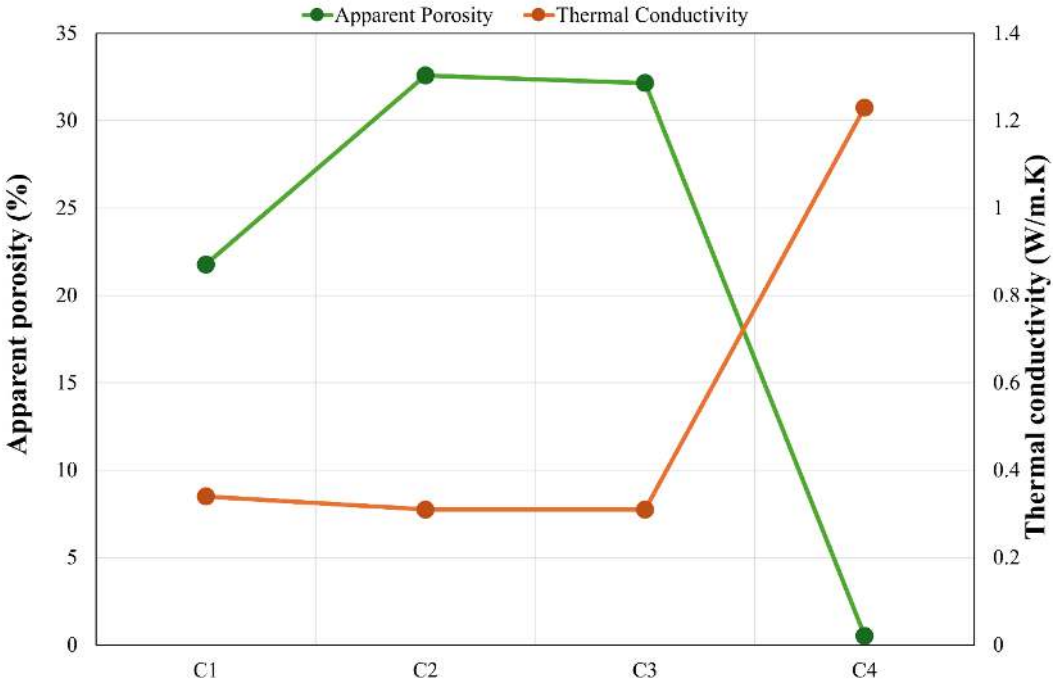

Figure 3.8 Apparent porosity against thermal conductivity

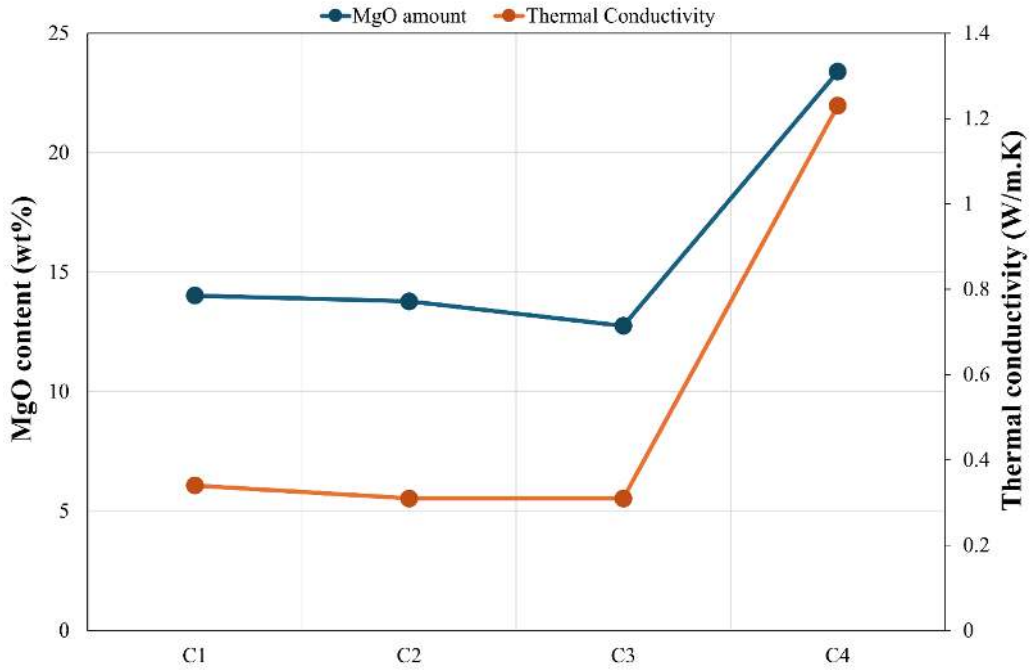

Figure 3.9 Thermal conductivity against MgO content

The flexural strength of the cordierite ceramic samples was calculated according to Equation 2.5 and listed in Table 3.3. C1 had the lowest flexural strength value, 43.19 MPa, whereas C4 had the highest value, 73.38 MPa. What influences the flexural strength of cordierite ceramics can be Al_2O_3 content, open porosity, and bulk density which are dependent on each other. As the porosity decreases, bulk density increases as well as flexural strength. Kuscer et. at. proved the correlation between density and flexural strength. They stated that density had a huge influence on flexural strength and cordierite ceramics with higher porosity had lowest flexural strength values [11]. Xu et. al. observed the effect of Al_2O_3 content on the mechanical properties of cordierite ceramics. Results showed that, until a certain amount of increase in Al_2O_3 content, porosity was also increased. However, bending strength showed an unexpected tendency where it increased with raising apparent porosity. After a certain amount of Al_2O_3, porosity and bending strength decreased. This situation might be caused by the pore shape and crystal size since longitudinal pores were expected to absorb fracture energy and increasing in crystal size resulted in the enhanced bending strength [21]. In another study where effect of excess MgO was observed in cordierite ceramics, the bending strength of the samples were measured

between 25-50 MPa. Also, it was observed that increasing the MgO content had no influence on bending strength of cordierite ceramics [32]. In this study, flexural strength increased with increasing porosity for compositions C1, C2, and C3. Only C4 showed opposite behavior with lowest porosity amount and highest flexural strength among the compositions. Figure 3.10 shows the comparison of open porosity and flexural strength for each composition. This situation can be explained with the minor phases present in C1, C2, and C3. As mentioned above, corundum phase was the secondary phase in these samples. The flexural strength of corundum ranges between 275-700 MPa which is extremely high compared to the cordierite ceramics whose flexural strength is 70-80 MPa [17]. Additionally, mullite was spotted as a minor phase in C1, C2, and C3. Mullite also have higher flexural strength than cordierite, 185 MPa [17]. The presence of corundum and mullite might cause an increase in C1, C2, and C3 despite their high porosity amount.

Table 3.3 Mechanical properties of samples

Sample	**3-point bending strength (MPa)**
C1	43.19 (± 7.79)
C2	55.84 (± 10.30)
C3	51.15 (± 3.05)
C4	73.38 (± 8.20)

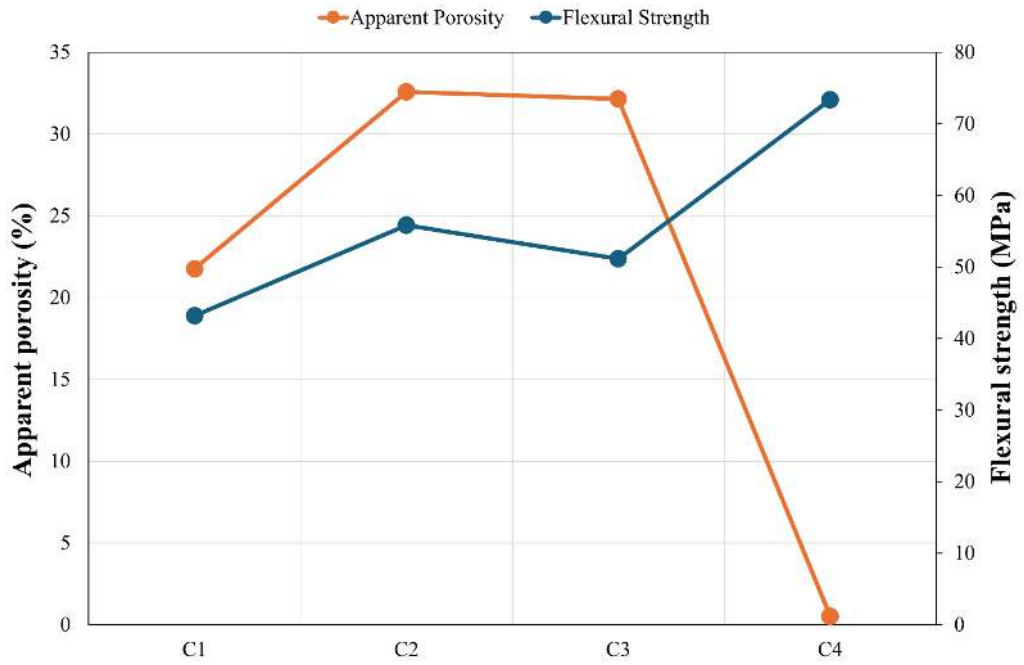

Figure 3.10 Apparent porosity vs Flexural strength

The dielectric constants and quality factors of the samples were calculated according to the Equation 2.6 and 2.7, respectively, and represented in the Table 3.4. Measured dielectric constant values were in the range of standard dielectric constant values of cordierite ceramics and they decreased as the frequency increased from 0.001 MHz to 5 MHz. There are several factors affecting the dielectric constant. Wing et. al. stated that as the porosity increased the dielectric constant decreased whereas dielectric loss increased. Also, humidity presence in the porous dielectric materials caused higher dielectric loss. Larger pores had higher influence to decrease dielectric loss than smaller pores as a result of free surface area reduction [39]. In another study, fully dense TiO_2 possessed extremely high loss factor due to lack of oxygen. That means, samples with closed pores had very low (<2000) Q value. Besides, it was shown that large grains resulted in higher dielectric loss [40]. Banjuraizah et. al. observed the influence of MgO mole ratio on dielectric properties of cordierite ceramics. They resulted that, dielectric constant decreased as frequency increased due to weakening of ionic polarization. Dielectric constant values were ranging between 5-7.5 and increased with MgO addition and forsterite formation since the dielectric constant of forsterite is higher than cordierite. Dielectric loss was also

increased with the amount of MgO mole ratio [24]. In this study, dielectric constant ranged between 3.78-5.30 which was similar to the standard value. As the porosity decreased, the dielectric constant increased as well. Figure 3.11 shows how dielectric constant changes depending on the frequency. Moreover, the phases present influenced the dielectric values. Indicated phases, mullite, forsterite, and corundum, have higher dielectric constant values, 6.6, 6.7, and 9.9, respectively, compared to the cordierite [25]. Dielectric loss decreased with increasing bulk density. C4 showed lowest tanδ factor among the samples. Less porosity resulted with less humidity and decreased loss factor while increased Q. C2 with stoichiometric composition and C4 had second lowest tanδ factors whereas C1 and C3 almost overlapped as shown in the Figure 3.12.

Table 3.4 Dielectric constants and loss factors of the samples

Frequency (MHz)	**Dielectric constant**				**Loss factor (tanδ)**			
	C1	**C2**	**C3**	**C4**	**C1**	**C2**	**C3**	**C4**
0.001	4.49	3.87	3.88	5.30	0.012	0.008	0.005	0.004
0.01	4.43	3.83	3.84	5.26	0.006	0.004	0.006	0.003
0.1	4.41	3.82	3.82	5.24	0.004	0.003	0.004	0.003
1	4.38	3.81	3.79	5.23	0.004	0.003	0.004	0.003
5	4.36	3.97	3.78	5.21	0.005	0.004	0.005	0.004

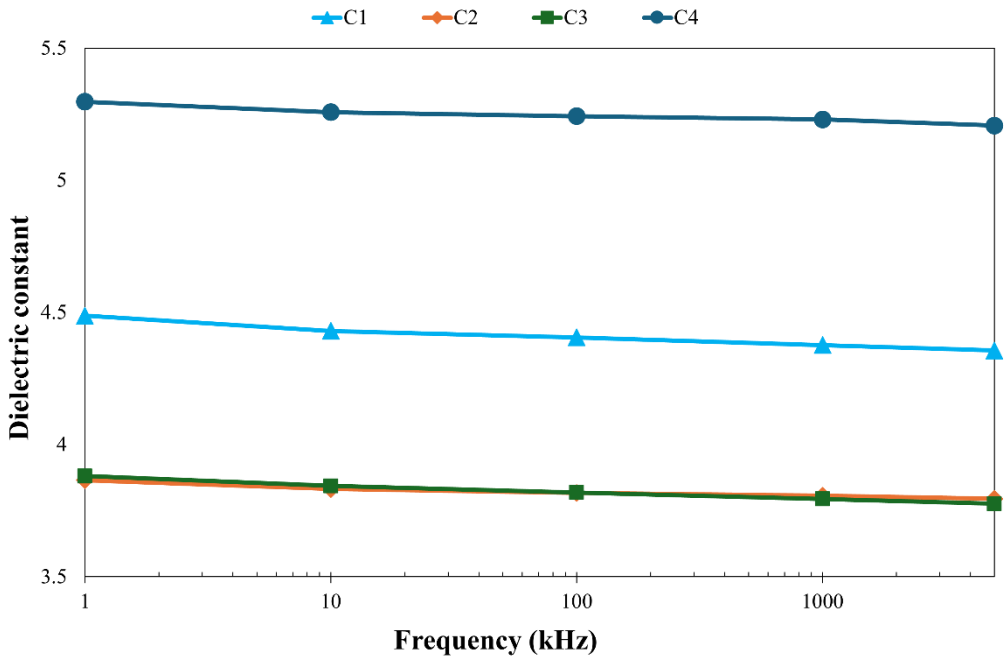

(a)

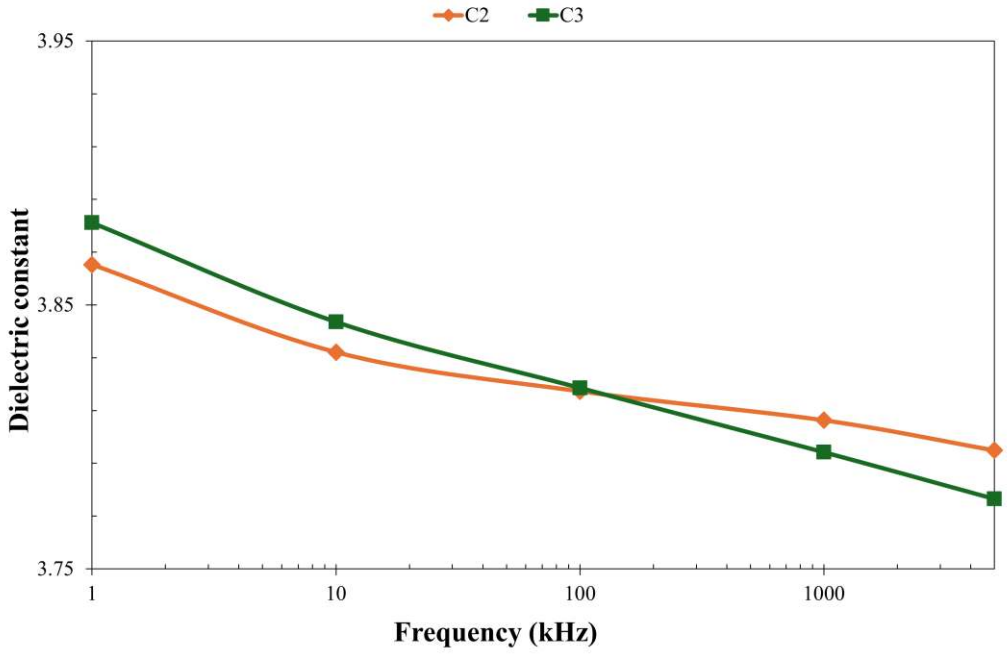

(b)

Figure 3.11 (a) Dielectric constant vs Frequency (1-5000 kHz) for C1, C2, C3, C4, **(b)** Dielectric constant vs Frequency (1-5000 kHz) for C2 and C3

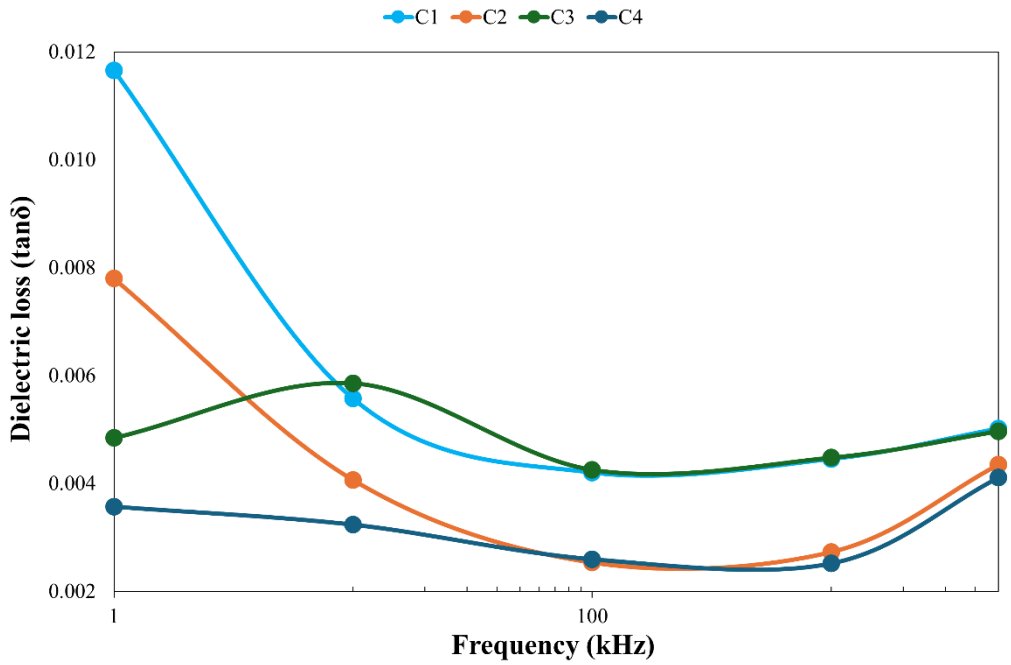

Figure 3.12 Dielectric loss (tanδ) vs Frequency (1-5000 kHz)

3.4 Effect of Composition on Microstructure

The lower and higher magnification SEM images of samples are presented in Figure 3.13 (a-f). The first three samples (Figure 3.13 (a-e)) have similar microstructural features. Strong neck formation between grains shows densification occurred in these samples via liquid phase. Also, pores and grains with rounded shapes proved that the solution-precipitation mechanism occurred during densification. However, the presence of porosity with interconnected characteristics demonstrates that both the amount and viscosity are insufficient so full consolidation cannot be achieved [41,42]. The higher magnification images (Figure 3.13 (b, d, f)) show that pore size is in micron-scale, and they show interconnected characteristics. The effect of liquidus temperature can be seen from SEM images of C4 (Figure 3.13 (g-f)). By decreasing of solidus and liquidus temperature, pore closure took place and closed pores formed due to increasing amount of liquid phase and reduction in the viscosity. The liquid phase volume became fairly large to fill up the porosity and accompanied pore closures. Figure 3.13 (f) demonstrates pores are completely isolated, they remain as closed porosity.

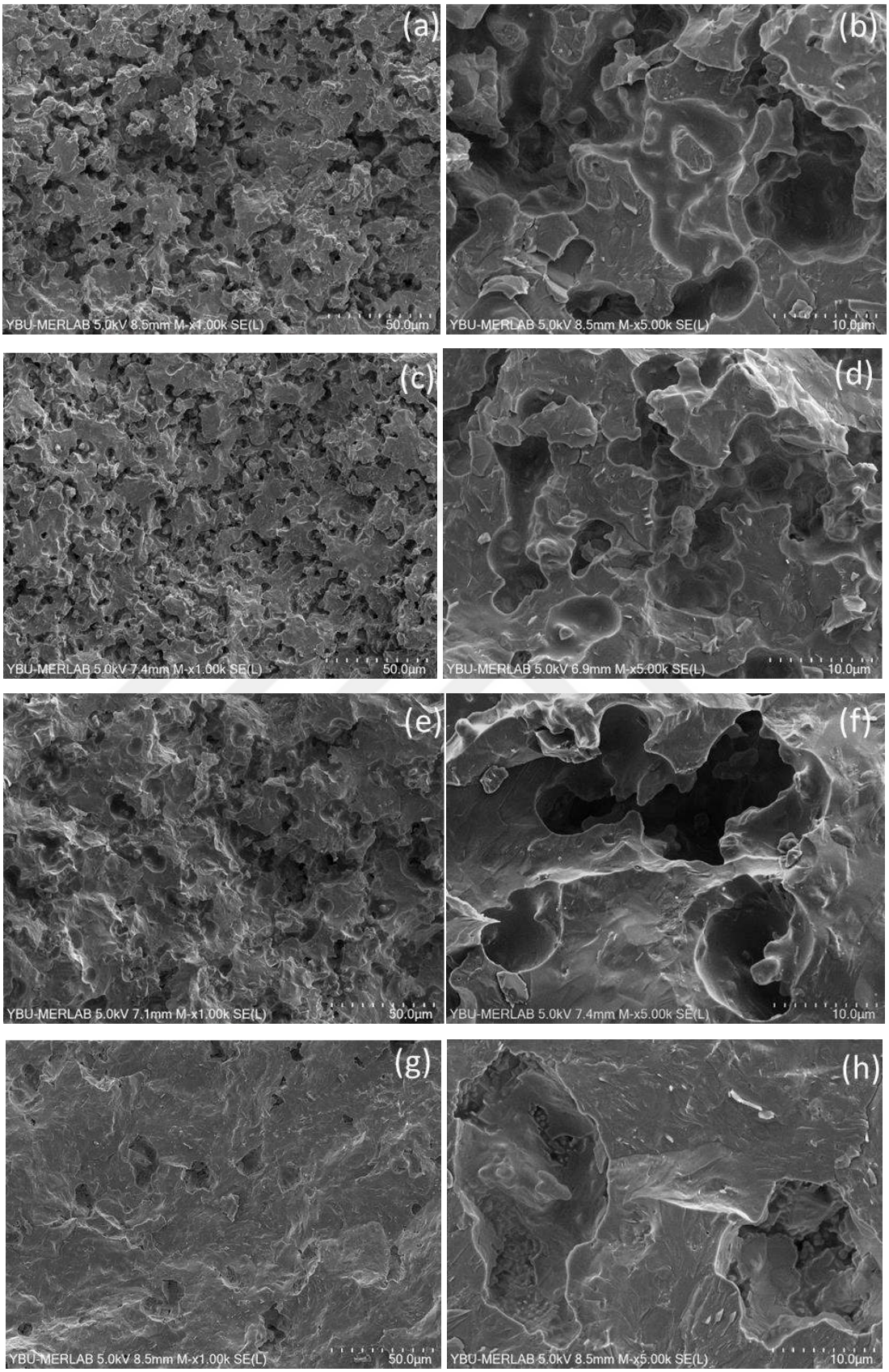

Figure 3.13 Microstructures of samples (a)-(b) C1, (c)-(d) C2, (e)-(f) C3, (g)-(h) C4

Figure 3.14 shows EDX elemental mapping of all the samples. All samples show homogeneous distribution in general. The elemental dispersion in C1, C2, and C3 (Figure 3.15 (a-c)) proves obtained phases. In the elemental mapping of C4 (Figure 3.15 d), except Al, all other elements had uniform distribution in the structure. In some regions which are indicated by white circles, a trace amount of Al was detected. On the contrary, the concentrations of Mg and Si were higher which proves formation of enstatite and forsterite phases in C4. The elemental analysis of the samples can be seen in Table 3.5. The highest Mg and lowest Al amount in C4 sample proved a sintering process without any loss. The ratios are similar to the compositions determined at the beginning of the process.

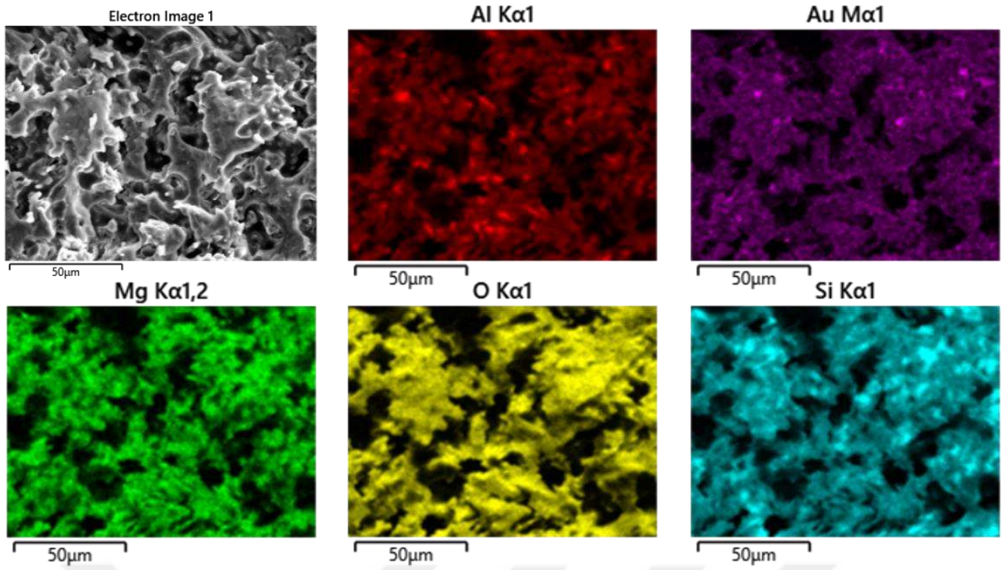

(a)

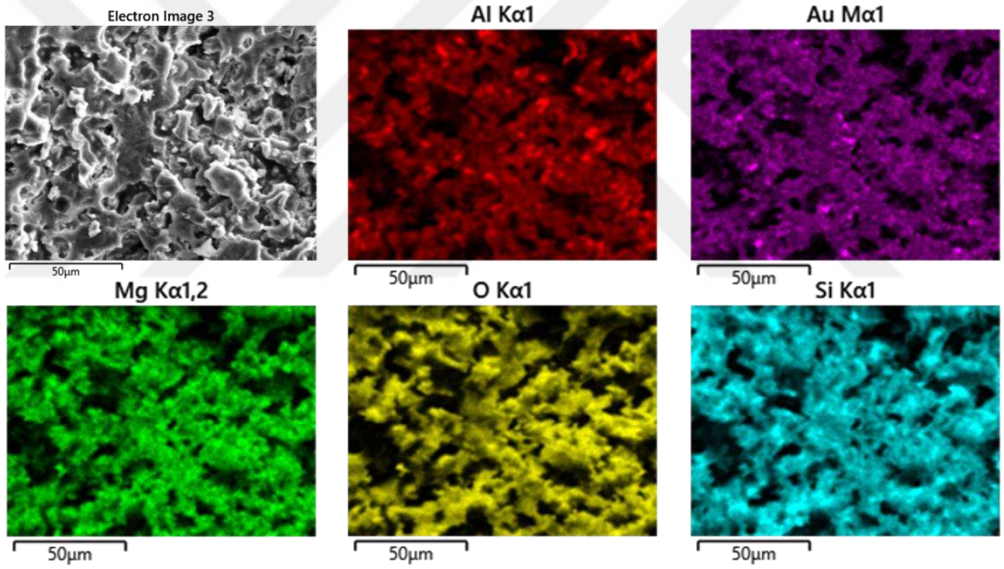

(b)

Figure 3.14 EDX mapping of (a) C1, (b) C2, (c) C3, and (d) C4

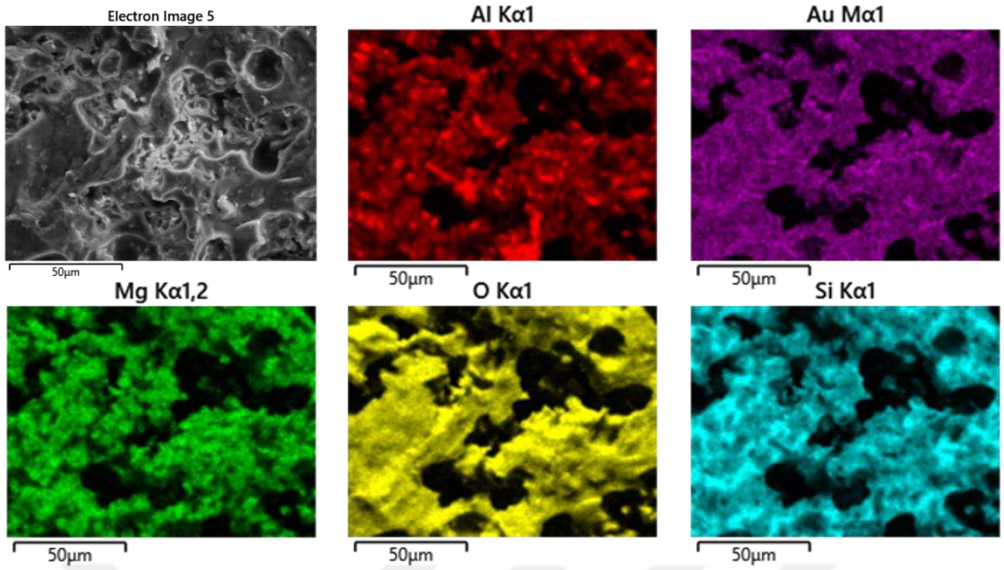

(c)

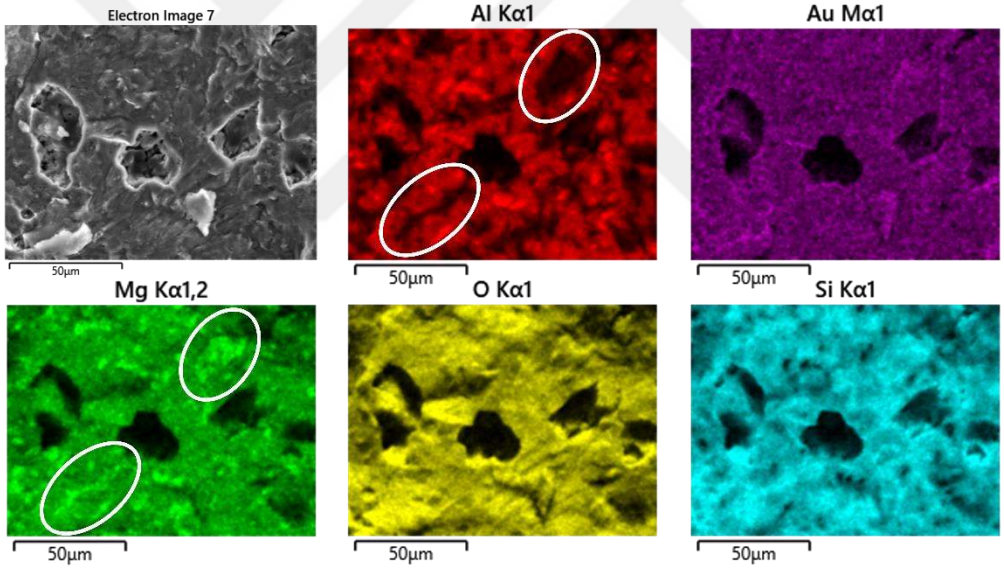

(d)

Figure 3.14 (continue) EDX mapping of (a) C1, (b) C2, (c) C3, and (d) C4

Table 3.5 Elemental analysis of the samples

Composition	O	Mg	Al	Si	Au	Total
C1	45.99	6.06	16.29	27.64	4.02	100.00
C2	43.42	5.98	18.12	25.77	6.71	100.00
C3	44.81	5.38	17.40	26.48	5.93	100.00
C4	43.35	9.36	14.00	27.20	6.09	100.00

CHAPTER 4

CONCLUSIONS

Cordierite ceramics ($Mg_2Al_4Si_5O_{18}$) is one component of the $MgO - Al_2O_3 - SiO_2$ ternary phase diagram. Its outstanding electrical and thermal properties make them a suitable material for certain electrical-electronics and thermal applications. Cordierite ceramics present low thermal expansion coefficient and dielectric constant, high thermal and chemical stability, excellent thermal shock resistance and electrical resistivity, low density, and moderate mechanical properties. However, sintering temperature range of cordierite is quite narrow which make sintering process challenging and decrease density and mechanical properties. It was proved that solidus and liquidus temperatures have significant effect on densification and final properties. Liquidus and solidus temperature difference must be high in order to increase the sintering temperature of the materials.

In this thesis, cordierite ceramics with low sintering temperature and high density were aimed to be produced by using the information from the $MgO - Al_2O_3 - SiO_2$ phase diagram. By choosing the reasonable composition points from the cordierite region in the phase diagram, ideal compositions were tried to be achieved. 4 compositions with low liquidus and solidus temperatures were selected and their difference kept high as much as possible. Lowering these temperatures by increasing MgO amount compared to the stoichiometric composition decreased the crystallization temperature and provided higher densification. Low sintering and crystallization temperatures are very important for several applications.

C4 samples showed highest density (2.45 g/cm^3) and lowest open porosity (0.53 %) among the compositions. Also, highest firing shrinkage (21.90%) and weight loss (13.71%) were observed in C4. As the MgO content increased, density and firing shrinkage increased as well while open porosity decreased since MgO promotes liquid phase formation. Indialite phase formed in all the samples. In C1, C2, and C3 corundum and mullite formation was observed. Sapphirine was detected in C4 samples. Small amount of forsterite appeared as minor phase in all samples.

Highest thermal conductivity and thermal diffusivity were spotted in C4 samples as 1.23 W/m·K and 0.16 mm^2/s, respectively. Thermal conductivity values were in sequence with apparent porosity amounts where with increasing porosity, thermal conductivity decreased. Also, MgO addition increased thermal conductivity as well. As a result of 3-point bending test, C4 showed highest flexural strength, 73.38 MPa as a result of low apparent porosity. Other samples showed same trend with flexural strength due to the present phases with higher flexural strength. The dielectric constant of the samples ranges between 3.78-5.30 and increased with decreasing porosity. As a result of highest density, highest Q values observed in C4.

According to the SEM images, interconnected pores were detected in C1, C2, and C3 proving that samples were not fully consolidated. Closed pores were observed in C4 samples as a result of liquid phase sintering. Due to the lowering liquidus and solidus temperatures and MgO content pores closed and isolated.

To conclude, cordierite ceramics with high density and low sintering temperature were fabricated with the help of phase diagram. C4 composition possessed suitable results as indicated in the literature. Lower sintering temperature and one-step cordierite production process helped to save time and energy. Outstanding dielectric properties make current C4 cordierite composition a suitable material for specific areas such as insulators, high-frequency applications, and microwave applications. A cordierite ceramic developed with these properties can be used as radome due to its low dielectric loss, or it can be used as an integrated circuit board as a result of its high dielectric constant. Further studies can be conducted by improving process parameters and characterization techniques.

REFERENCES

[1] Topateş, G. Farklı Magnezyum Kaynaklarından Kordiyerit Üretimi. Unpublished master's dissertation, Anadolu University. February, 2003.

[2] Rankin, G.A., Merwin, H.E. The Ternary System MgO-Al2O3-SiO2. The American Journal of Science, (*45*), 300. 1918

[3] Benito, J.M. et al. Cordierite synthesis. A time-resolved neutron diffraction study. Journal of the European Ceramic Society, (*32*), (2) 371. 2012

[4] Valášková, M. Clays, Clay Minerals and Cordierite Ceramics-A Review Vol. 59 2015 331–340 pp.

[5] Reda, A.E., Abd-El-Raoof, F., Ahmed, S.E., Abdel Aziz, D.A., Mahani, R. Sintering and dielectric behavior for doped cordierite by xCuO within MgO (1-x)–Al2O3–SiO2 ceramics. Materials Chemistry and Physics, (*243*), 2020

[6] Saheb, N., Lamara, S., Sahnoune, F., Hassan, S.F. Kinetics of α-cordierite formation from nano-oxide powders. Ceramics International, (*48*), (16) 23921. 2022

[7] Goren, R., Gocmez, H., Ozgur, C. Synthesis of cordierite powder from talc, diatomite and alumina. Ceramics International, (*32*), (4) 407. 2006

[8] Hou, Q., Luo, X., Liu, X., Xie, Z. Preparation of cordierite powder by chemical coprecipitation-rotation evaporation and solid reaction sintering.

[9] Soltan, A.M.M. et al. Microstructure and phase composition of cordierite-based co-clinker. Ceramics International, (*44*), (6) 5855. 2018

[10] De Almeida, E.P. et al. Cordierite obtained from compositions containing kaolin waste, talc and magnesium oxide. Ceramics International, (*44*), (2) 1719. 2018

[11] Kuscer, D., Bantan, I., Hrovat, M., Malič, B. The microstructure, coefficient of thermal expansion and flexural strength of cordierite ceramics prepared from alumina with different particle sizes. Journal of the European Ceramic Society, (*37*), (2) 739. 2017

[12] Chowdhury, A. et al. Synthesis, Properties and Applications of Cordierite Ceramics, Part 1 Vol. 18 2007

[13] Oliveira, F.A.C., Fernandes, J.C. Mechanical and Thermal Behaviour of Cordierite-Zirconia Composites

[14] Lou, W. et al. Low permittivity cordierite-based microwave dielectric ceramics for 5G/6G telecommunications. Journal of the European Ceramic Society, (*42*), (6) 2820. 2022

[15] Saeedi Heydari, M., Ghezavati, J., Abbasgholipour, M., Mohammadi Alasti, B. Various types of ceramics used in radome: A review. Scientia Iranica, (*24*), (3) 1136. 2017

[16] Massalski T.B., Laughlin D.E. Reference Module in Materials Science and Materials Engineering. Ed: Hashmi Saleem, Ed Elsevier, Oxford 2017 1–14 pp.

[17] Callister, W.D., Rethwisch, D.G. Materials Science and Engineering: An Introduction Wiley 2020

[18] Bergeron, C.G., Risbud, S.H. Introduction to phase equilibria in ceramics. 1984

[19] Carter, C.B., Norton, M.G. "Equilibrium Phase Diagrams" Ceramic Materials: Science and Engineering (CARTER, C.B., NORTON, M.G., Eds) Springer New York, New York, NY (120. 2007) 120–136

[20] Smith, A.L., Konings, R.J.M. Reaction kinetics and chemical thermodynamics of nuclear materials. Advances in Nuclear Fuel Chemistry, 3. 2020

[21] Xu, X., Lao, X. Effect of MgO/SiO2 ratio and Al2O3 content on crystallization behavior and properties of cordierite-based glass–ceramics. Journal of the European Ceramic Society, (*41*), (2) 1593. 2021

[22] Li, Y., Cheng, X., Zhang, R., Wang, Y., Zhang, H. Effect of excess MgO on the properties of cordierite ceramic sintered by solid-state method. International Journal of Applied Ceramic Technology, (*12*), (2) 443. 2015

[23] Li, Y., Qian, H., Cheng, X., Zhang, R., Zhang, H. Fabrication of dense cordierite ceramic through reducing Al 2O3 mole ratio. Materials Letters, (*116*), 262. 2014

[24] Banjuraizah, J., Mohamad, H., Ahmad, Z.A. Thermal expansion coefficient and dielectric properties of non-stoichiometric cordierite compositions with excess MgO mole ratio synthesized from mainly kaolin and talc by the glass crystallization method. Journal of Alloys and Compounds, (*494*), (1–2) 256. 2010

[25] Banjuraizah, J., Mohamad, H., Ahmad, Z.A. Effect of excess mgo mole ratio in a stoichiometric cordierite (2MgO·2Al2O3·5SiO2) composition on the phase transformation and crystallization behavior of magnesium aluminum

silicate phases. International Journal of Applied Ceramic Technology, (*8*), (3) 637. 2011

[26] Hwang, S.P., Wu, J.M. Effect of Composition on Microstructural Development in MgO-Al2O3-SiO2 Glass-Ceramics. Journal of the American Ceramic Society, (*84*), (5) 1108. 2001

[27] Zu, Q. et al. Compositional effects on mechanical properties, viscosity, and crystallization of (Li2O, B2O3, MgO)-Al2O3-SiO2 glasses. Journal of Alloys and Compounds, (*728*), 552. 2017

[28] Hu, Y., Tsai, H.-T. Compositional effect on the crystallization of the cordierite-type glasses. Journal of Materials Science, (*36*), (1) 123. 2001

[29] ASTM Standard Test Method for Flexural Strength of Advanced Ceramics at Ambient Temperature https://www.astm.org/c1161-18.html

[30] Dursun, G. M. Alumina/Glass Composites for Low Temperature CoFired Ceramics (LTCC) and Radome Applications. Unpublished master's dissertation, Ankara Yıldırım Beyazıt University. June, 2018.

[31] Karamanov, A., Dzhantov, B., Paganelli, M., Sighinolfi, D. Glass transition temperature and activation energy of sintering by optical dilatometry. Thermochimica Acta, (*553*), 1. 2013

[32] Lao, X., Xu, X., Jiang, W., Liang, J., Liu, J. Effect of excess MgO on microstructure and thermal properties of cordierite ceramics for high-temperature thermal storage. Ceramics International, (*45*), (17) 22264. 2019

[33] De Almeida, E.P. et al. Cordierite obtained from compositions containing kaolin waste, talc and magnesium oxide. Ceramics International, (*44*), (2) 1719. 2018

[34] Obradović, N. et al. Reaction kinetics of mechanically activated cordierite-based ceramics studied via DTA. Journal of Thermal Analysis and Calorimetry, (*124*), 667. 2016

[35] Lamara, S., Redaoui, D., Sahnoune, F., Heraiz, M., Saheb, N. Microstructure, thermal expansion, hardness and thermodynamic parameters of cordierite materials synthesized from Algerian natural clay minerals and magnesia. Boletín de la Sociedad Española de Cerámica y Vidrio, (*60*), (5) 291. 2021

[36] Shimizu, T., Matsuura, K., Furue, H., Matsuzak, K. Thermal conductivity of high porosity alumina refractory bricks made by a slurry gelation and foaming method. Journal of the European Ceramic Society, (*33*), (15–16) 3429. 2013

[37] García, E., Osendi, M.I., Miranzo, P. Thermal diffusivity of porous cordierite ceramic burners. Journal of Applied Physics, (*92*), (5) 2346. 2002

[38] Li, H. et al. In-situ synthesis and properties of porous cordierite ceramics with adjustable pore structure. Ceramics International, (*46*), (10) 14808. 2020

[39] Wing, Z.N., Halloran, J.W. Dielectric loss in porous TiO2. Ceramics International, (*43*), (5) 4618. 2017

[40] Templeton, A. et al. Microwave dielectric loss of titanium oxide. Journal of the American Ceramic Society, (*83*), (1) 95. 2000

[41] Rahaman, M.N. Ceramic Processing and Sintering CRC press 2017

[42] Kang, S.-J.L. Sintering: Densification, Grain Growth and Microstructure Elsevier 2004